2017-05-01

# Modeling Three Dimensional Ground Reaction Force Using Nanocomposite Piezoresponsive Foam Sensors

Parker Gary Rosquist
*Brigham Young University*

# Modeling Three Dimensional Ground Reaction Force Using Nanocomposite Piezoresponsive Foam Sensors

Parker Gary Rosquist

A thesis submitted to the faculty of
Brigham Young University
in partial fulfillment of the requirements for the degree of

Master of Science

Anton E. Bowden, Chair
David T. Fullwood
Matthew K. Seeley

Department of Mechanical Engineering

Brigham Young University

# ABSTRACT

## Modeling Three Dimensional Ground Reaction Force Using Nanocomposite Piezoresponsive Foam Sensors



Parker Gary Rosquist
Department of Mechanical Engineering, BYU
Master of Science


Three dimensional (3D) ground reaction force (GRF) are an essential component for gait analysis. Current methods for measuring 3D GRF involve using a stationary force plate embedded in the ground, which captures the forces as subjects walk across the platform. This approach has several limitations, a few being: it can only capture a few steps at a time, it is expensive to purchase and maintain, it can't reflect forces caused by natural uneven surfaces, etc. Previous research has attempted to develop wearable force sensors to overcome these problems; however, these endeavors have resulted in devices that are expensive, bulky, and fail to accurately measure forces when compared to static force plates.

This thesis presents the implementation and validation of novel nanocomposite piezoresponsive foam (NCPF) sensors for measuring 3D GRF. Four NCPF sensors were embedded in a shoe sole at four locations: heel, arch, ball, and toe. The signals from each sensor were used in a functional data analysis (FDA) to develop a statistical model for estimating 3D GRF. The process of calibrating the sensors to model GRF was validated through a study where 9 subjects (4 females, 5 males) walked on a force-sensing treadmill for two minutes. Two approaches were used to model the GRF response. The first approach was based on functional decomposition of the data. Using a tenfold cross validation process a statistical model was developed for each subject with the ability to predict walking 3D GRF with less than 7% error.

The second approach used machine learning to model 3D GRF. Using the same walking data for the statistical models, an artificial neural network (ANN) was used to create subject-specific models that could predict walking 3D GRF with less than 11% error. The predictive capabilities of ANN were tested using a pilot study where a single subject performed a calibration procedure by running at seven different speeds for thirty seconds each on the force-sensing treadmill. This calibration data was used to train a model, which was then used to estimate vertical GRF (VGRF) for three additional running trials at randomly selected speeds from within the calibration range. The ANN model was able to predict VGRF for three running speeds after calibration with less than 4% error.

The use of NCPF sensors to estimate 3D GRF was shown to be a viable alternative to static force plates. It is recommended, in future work, that 3D GRF and subsequent sensor data be collected from a large sample of subjects to create a baseline of 3D GRF characteristics for a population that will enable a robust cross-subject model capable of performing real-time ground reaction force analysis across the general population, which will greatly benefit our understanding of human gait.



Keywords: nanocomposite, ground reaction force (GRF), artificial neural network (ANN)

ACKNOWLEDGEMENTS

I would like to thank my advisor, Dr. Bowden, for guiding and mentoring me throughout this project as well as Dr. Fullwood and Dr. Seeley for their constant support, advice, and encouragement. I would like to thank all of the students from the departments of Mechanical Engineering, Exercise Science, and Statistics who worked with me on this project and assisted me during the phases of data collection, processing, and analysis. Finally, I would like to thank my family and friends for their support and never-ending optimism, without which I could not have progressed to where I am today.

Funding for this research was provided by the National Science Foundation under grant numbers CMMI-1538447 and IIP-1549719. Any opinions, findings, and conclusions or recommendations expressed in this material are those of the author and do not necessarily reflect the views of the National Science Foundation.

## TABLE OF CONTENTS

## LIST OF TABLES

## LIST OF FIGURES

# 1 INTRODUCTION

This work represents the implementation and validation of novel wearable sensors for use in a mobile gait analysis system. Gait analysis requires the combination of kinetic, kinematic, and electromyography data to predict internal forces and torques during ambulation. Kinetic data has been shown to contain many variables useful for biomechanical analysis. Current clinical methods require a subject to perform an exercise on a static force plate in order to capture accurate kinetic information. This protocol has several downsides including: the cost of equipment, spatial restrictions for movement, an artificial testing environment, and limits in the amount of data that can be collected. These drawbacks have created a surge in the development and testing of wearable sensors for collecting kinetic data in a mobile setting.

Recent advances in the Brigham Young University (BYU) nanocomposites laboratory have led to the development of a new kind of force sensor that has shown advantages in estimating three dimensional (3D) ground reaction force (GRF). When nickel-coated nanoparticles are mixed with a polyurethane foam matrix, a quasi-piezoelectric phenomenon is observed when the foam is impacted; a voltage response is created by the foam upon impact. Utilizing this self-sensing feature, four of these nanocomposite piezoresponsive foam (NCPF) sensors were embedded into the sole of a shoe to estimate 3D GRF.

Several studies were performed to model 3D GRF using the voltage response from NCPF foam sensors. In the first study, a statistical approach using functional data analysis (FDA) was

used to develop a model that predicted 3D GRF with a high degree of accuracy. This same data was used in an artificial neural network (ANN) modeling approach where models were developed to predict 3D GRF with comparable accuracy. An additional study required a single subject to perform a calibration protocol in a lab using a force-sensing treadmill, and then perform supplementary exercises that fit within the calibration range. The models produced by the ANN for this subject were able to predict vertical ground reaction force (VGRF) with a high degree of accuracy showing that a machine learning approach can allow for generalized predictions of VGRF within a subject.

NCPF foam sensors have been implemented and validated for estimating 3D GRF with a high degree of accuracy. The benefit of these sensors over alternative options is that they can perform a dual function: mechanical damping and producing a voltage upon impact. This allows the sensor to be embedded in a shoe where it can measure each step without interfering with the subject's natural gait. It is recommended that future work be done to gather a larger sample size of GRF data to characterize gait parameters across a population. Additional sensor development for measuring kinematic data can also be combined with these novel sensors to create a mobile gait analysis system. The importance of such a system can be explored by observing changes in gait parameters for people with degenerative disorders such as knee osteoarthritis.

Chapter 2 describes the background research that has been performed for developing a mobile gait analysis system. A brief history and description of gait analysis methods is explained. The variables of interest for 3D GRF are described along with the development of the NCPF sensors. A review of alternative wearable sensors is presented including their advantages and disadvantages. Finally, a description of statistical and machine learning approaches for modeling is given.

Chapter 3 describes the main work of this thesis in implementing and validating NCPF sensors for estimating 3D GRF. Nine subjects were recruited to walk on a force-sensing treadmill for two minutes while simultaneously collecting GRF and sensor data. A tenfold cross-validation process was used to build a model capable of estimating 3D GRF with a high degree of accuracy, and their results are discussed. This chapter is currently under review for publication as a peer-reviewed journal article. Co-authors on this paper are Gavin Collins, A. Jake Merrell, Noelle J. Tuttle, James B. Tracy, Evan T. Bird, Matthew K. Seeley, David T. Fullwood, William F. Christensen, and Anton E. Bowden.

Chapter 4 describes the ANN models used to estimate 3D GRF and the results they produced. Multi-subject walking data from Chapter 3 was used to train ANN models, which were able to predict 3D GRF with comparable accuracy to the statistical models. An additional pilot study involving one subject was carried out where a variety of running and walking speeds were performed on a force-sensing treadmill to create a generalized model for the subject. This model was then used to estimate VGRF curves and characteristics for three different exercises performed after calibration. The ANN results from both studies are discussed and compared to results from Chapter 3.

Chapter 5 concludes this thesis and suggests future research that can be done to build on this work and help develop a mobile gait analysis system.

# 2 BACKGROUND

## 2.1 Gait Analysis History

Gait analysis is the characterization of human ambulation. This complex movement has been researched intensively for hundreds of years and with the advent of new technologies, it is now becoming easier to understand. Starting with Aristotle and carrying through the Renaissance, scientists began an attempt to understand and describe the mechanics of walking [1]. By the early 1800's a description of the gait cycle was published through the work of the Weber brothers [2, 3]. Towards the end of the 19$^{th}$ century, researchers such as Braune and Fischer had begun to examine the mechanics of walking as well as analyzing the forces involved through the use of Newtonian mechanics [2, 4]. Research on the gait cycle significantly increased throughout the 20$^{th}$ century, especially as new technologies (e.g. force plates, electromyography, video recording, etc.) were developing. From these earlier studies a vast array of knowledge has been formed around human gait such as the transfer of energy throughout the gait cycle [5], muscle activity during walking [6, 7], joint forces during walking [8], and the movement of the center of gravity during walking [9-11].

The development of gait analysis techniques has culminated in its clinical applications for diagnosing and treating diseases. By understanding how normal gait should be presented during walking, deviations in gait caused by diseases can now be characterized. Clinicians have begun to distinguish gait patterns for several neuromuscular disorders such as cerebral palsy [12-14],

muscular dystrophy [15-17], multiple sclerosis [18], osteoarthritis [19], stroke [20, 21], chronic lower back pain [22], and Parkinsonism [23]. Not only can diagnosis be performed through gait analysis but it has also been studied as a possible tool for treatment and therapy [24].

## 2.2 Ground Reaction Force (GRF) Characteristics

Gait analysis uses motion, force, and electromyography data to understand the forces present in the body during movement. Kinetic data collected from force transducing sensors, such as static force plates, are used to identify the external forces required for joint movement [25]. Kinematic data collected from motion capture cameras and reflective markers are used to identify the trajectory of joint movement [26, 27]. With kinematic and kinetic data, an inverse dynamic approach can then be used to determine internal forces and torques within the body. These forces represent the net force acting across a joint; however, to understand which individual muscles contribute to this force, electromyography (EMG) data are collected from sensors applied externally on the skin or in vivo [28].

Kinetic data, in particular, have been shown to contain useful information for biomechanical analytics. The external forces applied during movement are known as three dimensional (3D) ground reaction force (GRF). By common convention, the directions of these forces are defined along the X axis (Anterior-Posterior), Y axis (Mediolateral), and the Z axis (Vertical). As researchers have studied different aspects of GRF curves (e.g. peak force, impulse, loading rate, stance time, strike pattern, etc.), important biomechanical information has been discovered. The correlations between 3D GRF characteristics and biomechanical factors can be used to help us understand what changes should be made in order to reduce the risk of injury.

Peak vertical ground reaction force (VGRF) was a characteristic of interest in lower limb stress fracture studies. Popp et al. investigated differences in bone strength and peak VGRF for

women with or without a history of stress fractures [29]. In this study, the bone strength and VGRF were measured for women during a long distance run; the women were classified as either having a history of stress fractures or not. The authors found that peak VGRF was significantly higher and bone strength was significantly lower in women with a history of stress fractures. The conclusion from this study was that the decrease in bone strength and increase in peak VGRF found in women with a history of stress fractures puts them at a higher risk of re-injury. It was suggested that training an individual to change peak VGRF during running could be beneficial in preventing future injuries.

Crowell et al. used VGRF as a variable for reducing the risk of stress fractures in a study where gait characteristics were altered using visual feedback [30]. Subjects went through several training sessions where gait parameters linked to stress fracture injuries were visually shown to them as they ran. The runners would try to stay under a target threshold while running, which in turn retrained their gait pattern. At the end of the training period, it was found that peak positive acceleration of the tibia, vertical force impact peak (peak VGRF), and average vertical force loading rates were all reduced. This suggested that using a visual feedback system where gait parameters such as peak VGRF could be displayed, could help improve running form and thus reduce the risk of stress fractures.

Another key VGRF characteristic of interest is the location and magnitude of the impact peak, which helps identify the strike pattern of an individual and can be an indicator for long-term health. Peak VGRF and loading rates of different foot strike patterns were examined to determine whether technique could affect risk of injury [31]. In this study, it was found that the impact force and loading rate for VGRF was significantly higher in heel strike runners than in forefoot strike runners. The conclusion was that the forefoot strike technique might help reduce

future injury by minimizing the forces on impact. This same conclusion was reached in another study that examined the relationship between foot strike technique and injury rate in a collegiate cross-country team [32]. The foot strike pattern was identified for members, and a history of their injuries was collected. The results from a generalized linear model showed that strike technique correlated with repetitive injury rates, and that the heel strike runner's injury rate was two times greater than that of the forefoot strike runner's.

In addition to VGRF peak and strike pattern, VGRF impulse has been shown to be another important GRF characteristic in assessing patient health. When assessing patients recovering from anterior-cruciate ligament (ACL) reconstruction, it was found that a key indicator for re-injury was asymmetry between knee moments. A study performed by Dai et al. found that this asymmetry in knee moments correlated with an asymmetry in VGRF impulse [33]. Being able to predict knee moment asymmetries using VGRF impulse asymmetries, the authors suggested that a "single-axis force transducer with low cost and flexible testing locations may have the ability to monitor sagittal plane knee kinetic asymmetries during the rehabilitation progress, which would be expected to assist in optimizing patient outcomes and minimizing re-injury rates" [33]. VGRF impulses have also been shown to correlate with running economy. In a study of 16 recreational runners, it was found that the total vertical impulse and net impulse of the VGRF significantly correlated to the running economy of the runners [34].

The ability to correlate GRF characteristics to health factors in movement is a large motivation for collecting kinetic data in everyday situations. Current methods for kinetic data collection require subjects to perform exercises on a static force plate, which means that only one stance of movement data can be collected at a time. This has resulted in testing procedures taking hours of time to perform, while yielding a small sample of usable data for analysis. Adding in the

cost of the equipment required to collect the data, the cost of personnel with the required training to run the equipment, and the limited locations able to provide this assessment, you get an analysis method that is underutilized in clinical applications [35, 36] and fails to reflect gait in natural environments [14]. To overcome these deficiencies, a flood of new research is currently being performed on GRF collection using wearable sensors.

### 2.3 Ground Reaction Force (GRF) Estimation Using Wearable Sensors

The desire for mobile data collection has led to an increased use of wearable sensors in gait analysis research. Many types of sensors have been used for collecting kinetic information such as: accelerometers, capacitive sensors, force sensing resistors, pneumatic bladder systems, and mobile force plates. Custom sensor systems were often built to meet the research needs; otherwise, a commercial system was utilized. The diversity of sensors in use has created several advantages and disadvantages for collecting GRF data while producing a myriad of results.

The most common type of sensor used to measure 3D GRF in prior research has been pressure sensors. These sensors utilize any type of force transducer with a given area; when applied in a grid formation, these sensors detect direct pressure of the foot during the gait cycle [37]. A commercial pressure insole known as the Pedar-X® (Novel GmbH, Munich, Germany) was used in several studies as the source of kinetic data collection. Ramanathan et al. validated the accuracy and reliability of this insole sensor finding the results to be repeatable and qualified for mobile gait analysis [38]. Because of its usefulness as an insole force sensing system, two other studies were performed where it was used to collect 3D GRF data in a mobile gait analysis system. Khurelbaatar et al. used this sensor to estimate VGRF with a high degree of accuracy (error < 2.80%, r = 0.99) however; the GRF along the anterior-posterior axis (APGRF) and the mediolateral axis (MLGRF) had higher error and slightly smaller correlation (error = 19%, 9.1%;

r = 0.96, 0.97), respectively [39]. Rouhani et al. also tested the validity of collecting 3D GRF with this sensor finding strong correlations and low error ($R > 0.77$, error < 23.61) [40], which they then utilized further in a mobile gait analysis system to estimate lower limb kinetics. These results were again found reasonably accurate (ankle moments: $R > 0.89$) [41]. An alternative commercial insole utilizing capacitive sensors known as the Moticon OpenGo (Moticon GmbH, München, Germany) was used to estimate spatial gait parameters such as stance time and cadence [42]. Although not directly measuring GRF, the pressure signal was effective in determining these parameters with reasonable accuracy.

Custom-built pressure sensor insoles were also common among recent literature as opposed to using commercially available systems. Jacobs and Ferris used a pressure sensor enveloped in a pneumatic neoprene bladder to measure 3D GRF simultaneously as the volume of the bladder changed during the gait cycle [43]. The system (cost: $800.00 per shoe, weight: 257.80 g per shoe) produced sensor data which was input into an ANN to model 3D GRF. The results from this model produced estimates that contained less than 10% error for any of the three GRF directions. Crea et al. also developed a novel pressure insole using an array of optoelectronic force transducers to measure VGRF as can be seen in Figure 2-1 [44]; as pressure is applied over the transducers, the light emitting from a diode in the sensor is partially covered changing the voltage response. Tests of this novel insole revealed that the sensor data had a high correlation to the actual VGRF ($R > 0.87$), but also had a high error between predicted and actual curves (error > 54.24).

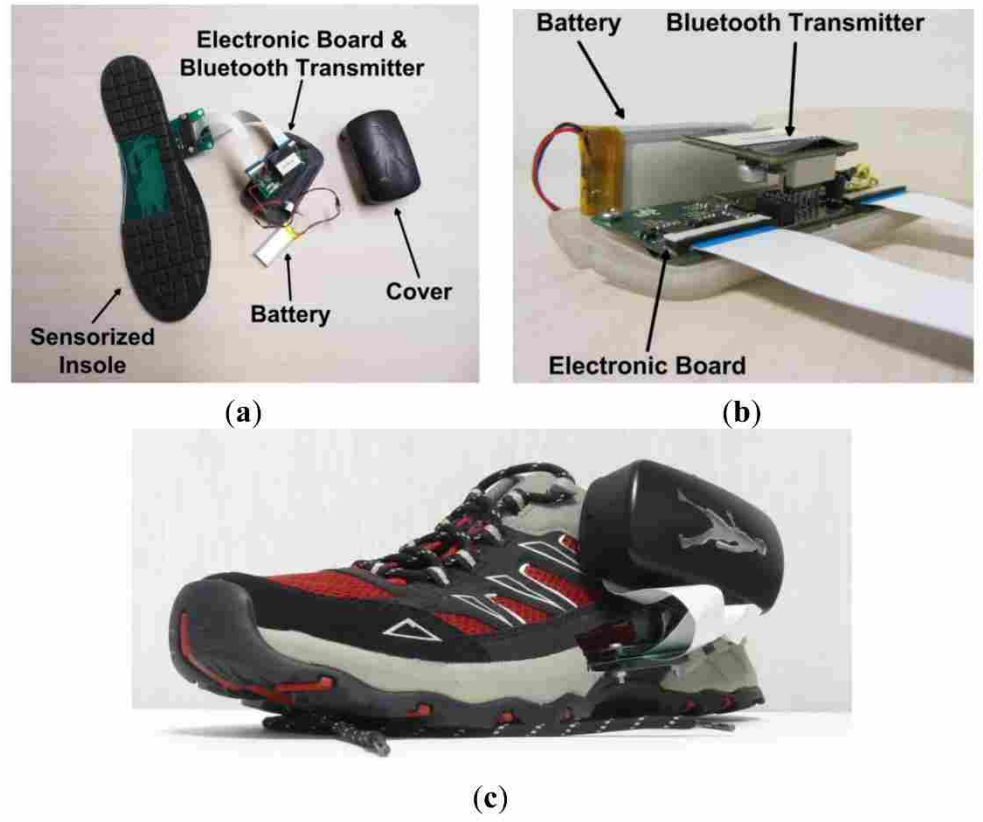


**Figure 2-1: Reprinted, with permission, from Crea, S., et al., A wireless flexible sensorized insole for gait analysis. Sensors vol. 14(1): p. 1073-1093 (2014).**

Several other studies used a system of force-sensitive resistors (FSR) to detect force temporally rather than spatially as was done with the pressure sensor insoles. Howell et al. developed an insole that contained 12 FSR to estimate VGRF and joint moments at the ankle, knee, and hip as can be seen in Figure 2-2 [45]. This insole system used linear regression models to estimate VGRF with a low error (5.4%) and obtained a high correlation for joint moments without any knowledge of limb position or spatial coordinates ($r > 0.80$). Gonzalez et al. also used a custom-built insole with FSR sensors; however, they used a non-linear modeling technique (fuzzy rule-based inference) to detect foot movement patterns [46]. This machine learning approach resulted in a model that classified 90% - 92% of the walking forward instances

correctly. An insole containing four piezoresistive force sensors was used by Minto et al. to measure spatiotemporal gait parameters [47]. As gait parameters were identified, haptic information was sent to the user via audio-tactile sensors to help adjust the user's gait showing potential for clinical rehabilitation applications.

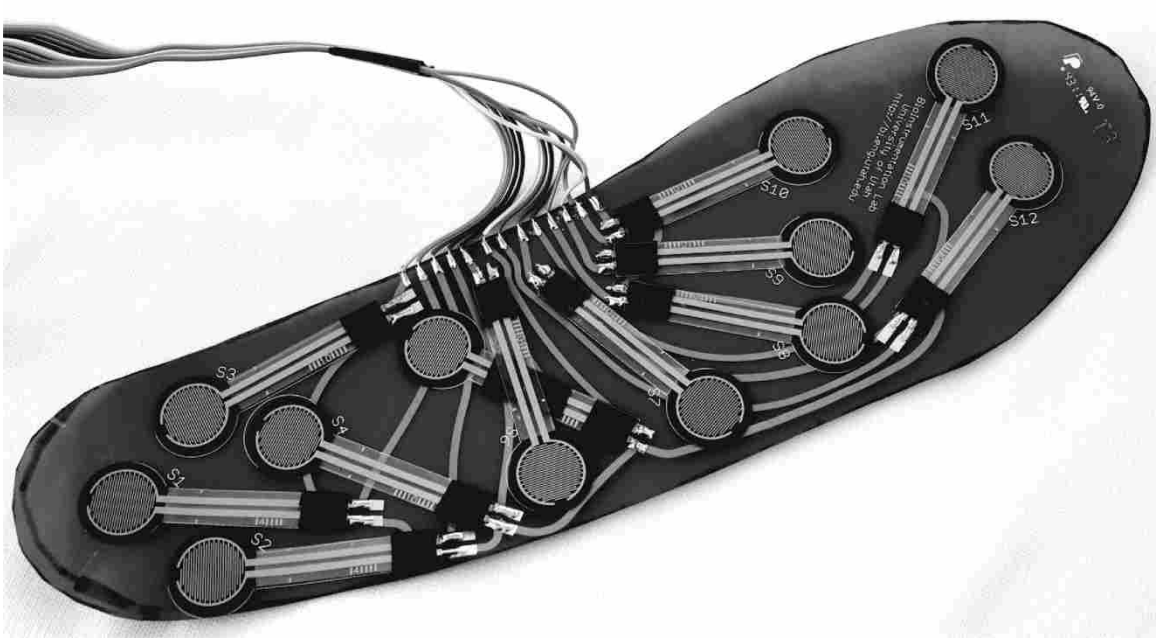


**Figure 2-2: Copyright © 2013 IEEE. Reprinted, with permission, from Howell, A.M., et al., *Kinetic gait analysis using a low-cost insole*. Biomedical Engineering, IEEE Transactions on, vol. 60(12): p. 3284-3290 (2013).**

Mobile force plates have been used as an alternative to pressure or piezoresistive sensors in order to provide a more direct measurement of force. Liu et al. attached two mobile force plates externally to the heel and forefoot locations of a shoe sole to estimate 3D GRF as can be seen in Figure 2-3 [48]. The instrumented shoe was able to detect GRF with a high degree of accuracy, where the root mean square differences between the sensors and the actual GRF along the X, Y, and Z axis were 5.1%, 6.5%, and 1.3%. These results encouraged the authors to use this sensor system in addition to inertial sensors to conduct a fully mobile gait analysis both in-

lab and out-of-lab [49]. Li et al. utilized this same mobile force plate system to estimate 3D GRF, but also attempted to input the sensor signals into an ANN to model joint angles [50]. The ANN model output was compared to joint angles measured by motion capture cameras and inertial sensors; the models created from the 3D GRF produced by the mobile force plates showed strong correlations to the knee and hip joint angles (R = 0.9), but a weaker correlation to the ankle angle (R = 0.7).

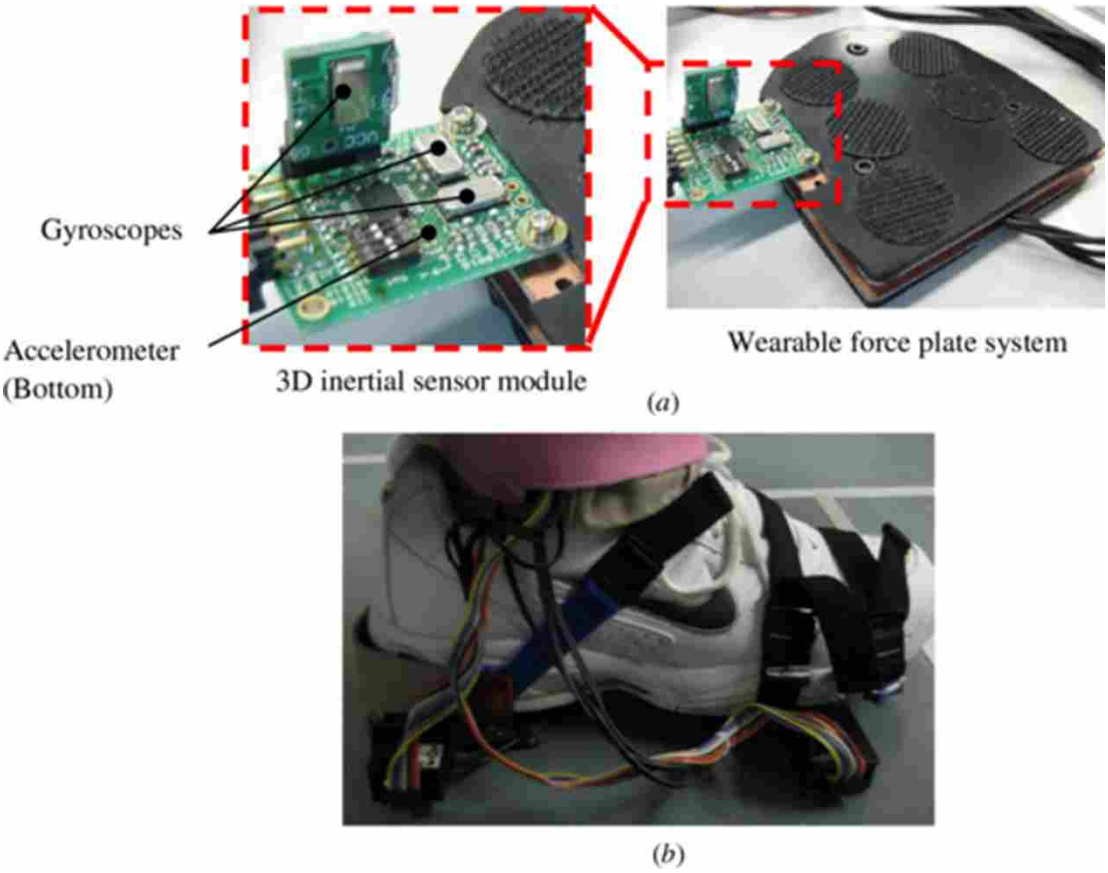


**Figure 2-3: Reprinted from Liu, T., Y. Inoue, and K. Shibata, *A wearable force plate system for the continuous measurement of triaxial ground reaction force in biomechanical applications*. Measurement Science and Technology, vol. 21(8): p. 085804 (2010). Copyright © IOP Publishing. Reproduced with permission. All rights reserved.**

An alternative method for collecting kinetic data without the use of any force transducing sensors has been to use kinematic data and an inverse kinematics approach to estimate 3D GRF.

Fluit et al. predicted 3D GRF and ground reaction moments (GRM) using kinematic data collected through motion capture software [51]. The results showed that residual forces and torques in the joints were significantly reduced when compared to using a static force plate. This method was also used to estimate 3D GRF during trunk bending by Faber et al. (Figure 2-4) with an average error of less than 20 N [52]. Oh et al. used this same approach combined with an ANN model to predict a single gait cycle of 3D GRF [53]. The resulting GRF estimates were highly accurate ($R > 0.917$) and the indeterminate problem found during the dual stance phase was resolved through the ANN model. The validation of this method shows that mobile gait systems utilizing inertial sensors to measure kinematic data [54] can estimate 3D GRF without the need for additional force sensors.

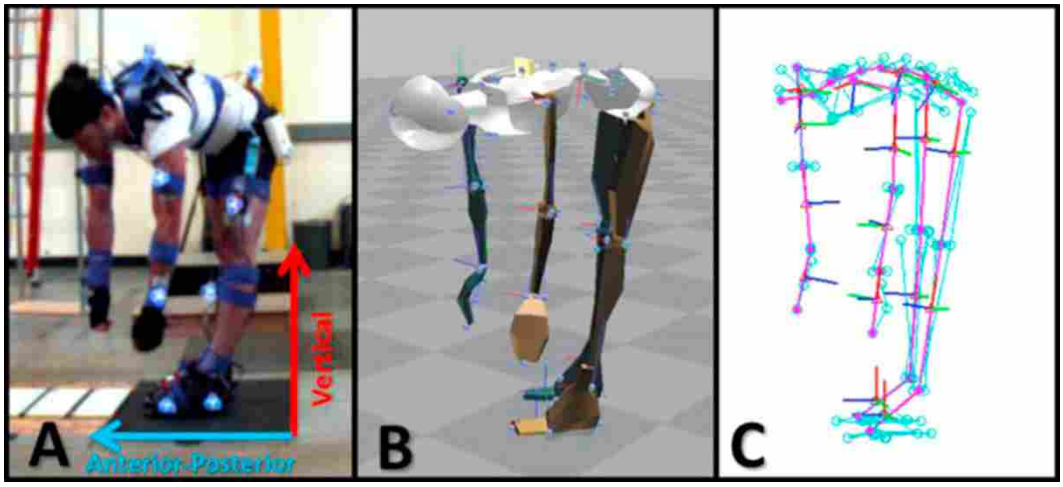


**Figure 2-4: System of inertial motion capture sensors and reflective markers for tracking spatial movement of limbs. Reprinted from Journal of biomechanics, Vol. 49(6), Faber, G., et al., *Estimating 3D L5/S1 moments and ground reaction forces during trunk bending using a full-body ambulatory inertial motion capture system*, p. 904-912., Copyright (2016), with permission from Elsevier.**

Although these wearable sensors have been shown to provide reasonably accurate results for a mobile gait application, they still fail to meet the needs of the user. In a review article by Bergmann and McGregor, the key elements that users identified in a wearable sensor were

compactness, embedded integration, and a user-friendly operation [55]. All of the pressure sensors were embedded in a shoe via the insole; however they presented problems such as a high cost to acquire [43] (e.g. commercial insole sensors), increased weight to the original shoe [43], and relatively high error between estimated GRF and actual GRF [44]. Studies using FSR sensors and mobile force plates presented a system that appeared bulky and cumbersome, requiring sensors, electronics, and wires to be externally attached to the subject along the shoe, ankle, knee, or hip [44, 46, 47, 49, 50]. This external application of sensors to the body outside of the shoe may inhibit natural gait and make users feel self-conscious when using them in a natural environment. Even studies trying to remove kinetic sensors altogether still require the attachment of inertial sensors directly to the body for motion capture, which may introduce higher error, require a complex setup, and interfere with normal movement [51-54]. A few of the results validating these sensors came from a single stance of data or a single type of ambulation (e.g. single speed of movement), which fails to recognize variability between stances or variability between speeds of movement [42, 52, 53]. Several of the studies performed used their sensors to only recognize spatiotemporal gait parameters rather than estimate GRF directly [42, 46, 47]; although spatiotemporal gait information can be useful, GRF estimates can be used determine these parameters as well as allow for an inverse dynamic analysis when coupled with kinematic data. The work done by these authors has shown that wearable sensors hold great potential for a gait analysis application; however, the high cost, large bulk, complicated attachment, and lack of accurate GRF estimations over a range of movements prevent these systems from being widely used in an out-of-lab application. A low-cost, low-weight sensor system needs to be developed to provide accurate GRF estimates for a variety of exercises, while being embedded in a way where interference with the body and gait of the subject is minimized.

## 2.4 Nanocomposite Piezoresponsive Foam (NCPF) Sensors

To meet the needs for a low-cost sensor system to measure 3D GRF, a new kind of sensor has been developed in the BYU Nanocomposites Research Lab. Previous work in this lab has been developing high deflection strain gauges by embedding nanocomposite fillers into a silicone matrix [56-58]. These sensors produced a piezoresistive effect under tensile strain, which has been utilized for biomechanical measurements [59]. It has been shown that adding carbon based nanofillers to a polyurethane foam increases the electrical conductivity of the material [60]. Recently discovered NCPF utilizes this same principle; however, nickel based nanofillers are used instead of carbon based nanofillers. This composite material exhibits a change in voltage upon compressive (negative) strains, making it an ideal application in high impact environments [61]. These foam sensors have been tested in football helmet pads to measure impacts during tackling, taekwondo chest protectors to measure the force of a kick to the sternum, and even as bushings to determine vibration frequencies in planetary mixers [62]. The benefits that these sensors provide over traditional force or strain sensors is that they are able to withstand large strains (> 50%) repeatedly, the material and manufacturing cost is very low, and the process to measure the voltage response is relatively simple and easy to implement. The dual nature of the foam to act as a sensor and energy absorber makes it ideal for applications where foam is normally used to absorb high-energy impacts (e.g. foam padding in shoes, helmets, athletic equipment, etc.).

To correlate the signal from these sensors to the forces applied, several approaches have been used including: physical, statistical, and machine learning models. Previous research has attempted to model the piezoresponsive behavior of nanocomposite sensors using either quantum tunneling [56], percolation [60], or a combination of both [59, 63]. Because the signal from the

NCPF sensors is quasi-piezoelectric (e.g. the voltage changes with strain) the behavior is different from previously designed composite sensors and thus an alternative method for modeling forces has been chosen. In this thesis, two different modeling techniques are compared for correlating sensor signals to GRF: statistical modeling (Chapter 3) and ANN modeling (Chapter 4). The statistical approach uses a functional data analysis (FDA) where a linear regression model is developed from Fourier coefficients [64]. The ANN model utilizes machine-learning algorithms to produce a non-linear model [65]. Other mobile gait applications have used linear regression models [45], ANN models [43, 50, 53], or both models [40] to estimate 3D GRF curves and parameters with reasonable accuracy.

The purpose of this thesis was to implement and validate an NCPF sensor system that can collect kinetic data and estimate 3D GRF with a high degree of accuracy. Previously developed insole sensors have had problems accurately estimating GRF parameters, while also being too expensive and complex for ease of use in a natural environment. The low-cost and dual function of NCPF sensors make them an ideal solution for a mobile gait analysis application. Being made from a composite foam material, these sensors can be easily embedded into the sole of a shoe where they will neither inhibit the gait of the user nor inhibit the function of the shoe. The signal generated by the sensors during ambulation was modeled and subsequently validated using both a statistical and an ANN approach in order to estimate 3D GRF with a high degree of accuracy.

# 3 ESTIMATION OF 3D GROUND REACTION FORCE USING NANOCOMPOSITE PIEZO-RESPONSIVE FOAM SENSORS DURING WALKING

## 3.1 Abstract

This paper describes a method for the estimation of the 3D ground reaction force (GRF) during human walking using novel nanocomposite piezo-responsive foam (NCPF) sensors. Nine subjects (5 male, 4 female) walked on a force-instrumented treadmill at 1.34 m/s for 120 s each while wearing a shoe that was instrumented with four NCPF sensors. GRF data, measured via the treadmill, and sensor data, measured via the NCPF inserts, were used in a tenfold cross validation process to calibrate a separate model for each individual. The calibration model estimated average anterior-posterior, mediolateral and vertical GRF with mean average errors (MAE) of 6.52 N (2.14%), 4.79 N (6.34%), and 15.4 N (2.15%), respectively. Two additional models were created using the sensor data from all subjects and subject demographics. A ten-fold cross validation process for this combined data set resulted in models that estimated average anterior-posterior, mediolateral and vertical GRF with less than 8.16 N (2.41%), 6.63 N (7.37%), and 19.4 N (2.31%) errors, respectively. Intra-subject estimates based on the model had a higher accuracy than inter-subject estimates, likely due to the relatively small subject cohort used in creating the model. The novel NCPF sensors demonstrate the ability to accurately estimate 3D GRF during human movement outside of the traditional biomechanics laboratory setting.

## 3.2 Introduction

Gait analysis is an essential tool in identifying and understanding human ambulation. The modeling of three-dimensional ground reaction forces (3D GRF) is an essential element of gait analysis [25]. GRF analysis can be used to identify key gait parameters such as cadence, heel strike, and toe off. The measurement of GRF now requires a subject to walk across a force plate which is either located in the floor or in some sort of moveable surface (e.g. treadmill or platform). Thus, commercial force platforms and treadmills are both expensive and stationary (i.e., can only be used in laboratory environments) [35]. Further, only a few steps can be recorded at a time using the aforementioned commercial force platforms, making data collection time-intensive and inefficient. Treadmills instrumented with force platforms can be used to collect more data; however, these treadmills cost approximately ten times more than a traditional force platform. Such a cost prohibits many researchers from obtaining treadmill GRF data. These issues have led to a technological push in the development of mobile force sensors, which could open new possibilities for applied gait analysis.

Considerable work has already been performed to estimate GRF using mobile force sensor systems. Several efforts have been made to predict GRF using full body kinematics [51, 53]. Inertial measurement sensors have also been used in similar fashion to replace the need for motion capture cameras in the prediction of GRF [52]. Mobile force sensors such as force sensing resistors [44, 45], portable tri-axial force plates [48, 66], pneumatic bladder systems [43], and commercial pressure insoles [38-40] have also been used to estimate GRF. Although these approaches have shown promising results, several limitations have been described, such as: dependency on anthropometric mass measurements [51-53], high cost to produce [43], bulky equipment that may interfere with natural gait [49], no estimate of anterior-posterior or

mediolateral GRF [44, 45], and large error when anterior-posterior and mediolateral GRF were reported [38-40].

Recent development of a novel piezo-responsive polyurethane foam has introduced a new kind of sensor that may provide accurate estimates of 3D GRF. In previous work, we observed that adding nickel-based nanoparticles to a silicone substrate causes the material to exhibit piezo-resistive properties [56]. The electromechanical behavior of these sensors has been validated for use in various large-strain applications [58, 59]. Additionally, when the same nanoparticles are added to a polyurethane foam substrate, the material displays a quasi-piezoelectric effect, where the material produces a voltage as it deforms [61]. The strain-induced voltage is measured by attaching a conductive material embedded in the foam (e.g. wires as shown in Figure 3-1) to a voltage measurement system, which correlates to the force of impact [61]. This quasi-piezoelectric response from a flexible material's signal has been correlated with both force and frequency in high deformation environments [67]. By embedding these sensors into a shoe sole, we hypothesize that the voltage response generated during gait will correlate to 3D GRF with a reasonable degree of accuracy.

In addition to its use in improving athletic performance, GRF has clinical applications in the diagnosis and treatment of various physical impairments (e.g., cerebral palsy [12-14], muscular dystrophy [15-17], multiple sclerosis [18], osteoarthritis [19], stroke [20, 21], chronic lower back pain [22], and parkinsonism [23]). Development of less-expensive, wearable sensors that can estimate a continuous amount of accurate GRF without restricting the subject to a confined path would provide researchers with a new tool for expanding the science of gait analysis to additional clinical, sports performance, and diagnostic applications [68]. This paper

provides testing and validation data for a shoe-mounted, NCPF sensor technology for estimating GRF with reasonable accuracy.

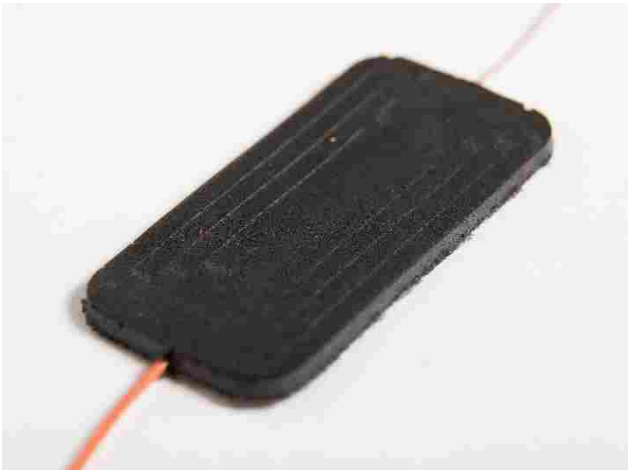

**Figure 3-1: Nanocomposite piezo-responsive foam (NCPF) sensor with wires embedded to measure the voltage response during impacts.**

## 3.3 Materials and Methods

Five healthy male subjects (age, 24.2 ± 2.2 yrs; height, 174.1 ± 6.5 cm; mass, 75.0 ± 8.1 kg; shoe size, US Men's 9.5) and four healthy female subjects (age, 23.5 ± 1.7 yrs; height, 167.5 ± 7.0 cm; mass, 57.8 ± 3.6 kg; shoe size, US Women's 8) volunteered to participate in this study (see Table 3-I). Subjects were recruited and followed protocol that was approved by the appropriate institutional review board. After a brief period of walking on the treadmill to help the subject become familiarized with the movement, the subject walked at 1.34 m/s, for 120 s, on a treadmill that was instrumented with two fore-aft force platforms (AMTI, Watertown, MA, USA).

**Table 3-I: Sex, age, height, and mass for each volunteer subject.**

| Subject | Sex | Age (yrs) | Height (cm) | Mass (kg) |
|---|---|---|---|---|
| **1** | F | 25 | 167.6 | 59.0 |
| **2** | M | 26 | 172.7 | 79.8 |
| **3** | F | 21 | 172.7 | 56.7 |
| **4** | M | 27 | 185.4 | 68.0 |
| **5** | M | 23 | 169.5 | 85.3 |
| **6** | M | 23 | 172.7 | 65.8 |
| **7** | M | 22 | 170.2 | 76.2 |
| **8** | F | 24 | 157.5 | 53.5 |
| **9** | F | 24 | 172.0 | 62.0 |

The sole of the right shoe was instrumented with a nanocomposite piezoresponsive foam (NCPF) sensor in four locations: heel, arch, ball, and toe (Figure 3-2). Each of the four NCPF sensors used in this study was made individually from a standard two-part polyurethane foam (AquaFlex 20702, Utah Foam Products, Inc.). 1-mm chopped nickel-coated carbon fiber and nickel powder (3% and 15% by weight, respectively) were mixed with isocyanate (A-side), and subsequently combined with polyol (B-side). This foaming mixture was poured into an aluminum mold to bind to the two wire leads (used to measure one signal of output voltage) and reach their desired geometry (25.4 x 50.8 x 3.3 mm). The foam cured for ten minutes on a hot plate (43°C) before being released from the mold and allowed to sit at room temperature for 24 hours to complete the curing process.

Although the present work is focused primarily on the accurate measurement of 3D GRF data, material characterization data performed in our laboratory for the NCPF is presented here to provide context, specifically with respect to the influence of temperature and cyclical strain on its performance. It was observed that voltage responses from the NCPF increase linearly with increased temperature, where voltage increases four mV for every one degree Celsius. Further,

cyclic testing (30,000 cycles) under simulated gait conditions (1335 N impacts at 1 Hz for 8 hour and 20 minute durations) resulted in a signal that exhibited a mean peak voltage response of 0.4 V and a signal to noise ratio of 50. The peak voltage decreased by 0.08 V over the duration of the 30,000 cycle test which resulted in a signal drift of 2.67 mV (0.00067%) per cycle. It was observed that the drift was temporary (signal returned to the original magnitude between repeated tests of the same NCPF sample), likely due to temperature. Compression tests producing stress-strain curves revealed that the NCPF sensors exhibit a Young's modulus (linear elastic region) of 377.7 kPa, a Plateau modulus (plateau region) of 6.1 kPa, and a plastic collapse stress of 7.3 kPa

Each sensor was wired to a microcontroller placed on top of the tongue of the shoe and held in place by the shoelaces (Figure 3-2). This microcontroller was powered using a 3.7 V 300 mAh lithium ion polymer battery. Although not a focus of this paper, power consumption tests were performed on a 105 mAh battery where it was shown that power was provided to the microcontroller for at least 6 hours without the voltage dropping below the 3.3 V minimum microcontroller requirement. The system of sensors, microcontroller, and battery increased the weight of the shoe by 8.36% or 25.5 grams at an estimated production cost of less than $75.

In order to synchronize the shoe sensors and GRF data, the subject would strike the force plate with the right heel, and then immediately remove the foot from the force plate to create a spike in the force data at the beginning of the test. This point of impact was then used to synchronize sensor and force plate data. After this strike, the subject then stepped onto the treadmill and walked at 1.34 m/s for 120 s.

Data were collected simultaneously from the force plates (GRFs), cameras, and NCPF sensors at 1000 Hz, 250 Hz, and 1029 Hz, respectively. MATLAB® (MathWorks™, Natick,

MA, USA) was used to downsample the sensor data to match the sampling rate of the force plates (1000 Hz) using an antialiasing finite impulse response, lowpass filter. Force plate and camera data were collected synchronously with the same clock; because the camera data was sampled at one-fourth the rate of the force plate data, no upsampling was necessary. The force plate data and reflective marker trajectories were exported to Visual 3D software (C-Motion Inc., MD, USA), where a model of each foot was created using the reflective marker position data; this foot model was only used to facilitate assignment of the GRF vector to the correct foot. Because heel strike and toe-off events were determined from the GRF data, the accuracy of the foot model did not have an effect on the accuracy of any subsequent data analysis. Next, in MATLAB®, the GRFs that were applied to the right foot and the sensor data were synchronized, using the aforementioned initial heel impact (as determined using the GRF data assigned to the right foot). To visualize the output signal from each sensor during walking, a representative graph of the aligned sensor data scaled to the magnitude of the force data for one stance phase. has been included in Figure 3-3.

Analysis of each subject's data set was performed using R software[69]. All GRF and sensor data were filtered using a low pass Butterworth filter (fourth order filter with a cutoff frequency of 21 Hz). The filtered data were then separated into individual stance phases (heel-strike to toe-off), and each of these stances phases was normalized such that there were 200 equally spaced data points per curve. As a final step, the sensor curves were approximated by Fourier series, each consisting of an intercept term, k sine terms, and k cosine terms, as shown in Equation 3-1,

$$\hat{s}_i(t) = \hat{\theta}_0 + \sum_{j=1}^{k} \hat{\theta}_j \sin(j\omega t) + \hat{\varphi}_j \cos(j\omega t) \tag{3-1}$$


**Figure 3-2: The shoe that was instrumented with the nanocomposite piezo-responsive foam sensors, microcontroller, and battery. The sensors were embedded under the insole at the heel, arch, ball, and toe positions and the reflective markers were placed at the heel, toe, and lateral positions for motion capture.**

where $\hat{s}_i(t)$ is the approximated heel, arch, ball, or toe sensor curve at time point $t$ in the $i^{th}$ stance, where $\hat{\theta}_0$ is the intercept term and $\hat{\theta}_j$ and $\hat{\varphi}_j$ are amplitudes of sine and cosine terms in the Fourier approximation, where $\omega$ is a constant equal to $2\pi$ divided by the number of data points in each stance, and where $k_.$ is both the number of sine and the number of cosine basis functions used to represent a voltage stance. In our case $\omega = \frac{2\pi}{200} = \frac{\pi}{100}$ and, for each subject, $k_h$, $k_a$, $k_b$, and $k_t$ are chosen to be the number of sine and cosine terms in the Fourier approximation of the heel, arch, ball, and toe sensor curves, respectively.

To estimate the 200 data points in each GRF curve, the $K = 4 + 2(k_h + k_a + k_b + k_t)$ amplitudes corresponding to the Fourier terms for the sensor signals were used as independent

variables in a multivariate regression analysis. In other words, our predicted values for GRF are linear combinations of these K sensor amplitudes.

For each subject, a separate variable selection process was used to choose the optimal numbers $k_h, k_a, k_b$, and $k_t$ of sensor amplitudes from each of the four sensors in order to accurately predict GRF in a cross validation setting. For each proposed model, 10% of the total stances (test set) were randomly removed, a model was built using the remaining 90% of the data (training set), GRF estimations were obtained for the test set, and the Mean Absolute Error (MAE) was calculated for these predictions. This process was iterated 1,000 times, choosing a different test set for every iteration, and the model with the lowest average MAE was chosen. This model, which we call the Single Subject (SS) model, was created as a calibration model to show that the voltage sensors are capable of estimating the GRF of a single subject.

A second model, which we call the Combined-Subject Voltage (CSV) model was created using a single data set of all subjects combined. For this analysis, the best combination of $k_h$, $k_a$, $k_b$, and $k_t$ were again chosen to minimize predictive error. A set of 1,000 ten-fold cross validation processes were again performed on each proposed model, with randomly selected subsets consisting of 10% of all stances acting as test sets to be predicted from the remaining combined-subject set of stances. The model with the combination of variables that minimized the error between the estimated and actual GRF curves was selected. This model was then used in another cross validation analysis, where the stances of one subject were removed (test set), a model was fit using data from the remaining eight subjects (training set), estimations were obtained for the GRF of the test subject, and MAE was calculated for these predictions. This process was repeated nine times, each time choosing a different subject to be the test subject.

A final model was created using the same data set of all subjects combined that was used in the second model, but subject demographics (age, height, weight, and gender) and the interactions between subject demographics and the K sensor amplitudes were also included – hence we call this model the Combined-Subject Voltage and Demographics (CSVD) model. A variable-selection process was again used to determine which subset of the demographics would minimize the error between predicted and actual GRF curves. Again, 1,000 ten-fold cross validation processes were performed on each of the possible models, and the model including the subject demographics that minimized average MAE was selected. This final model was also used in a cross validation analysis across subjects, similar to that of the second model.

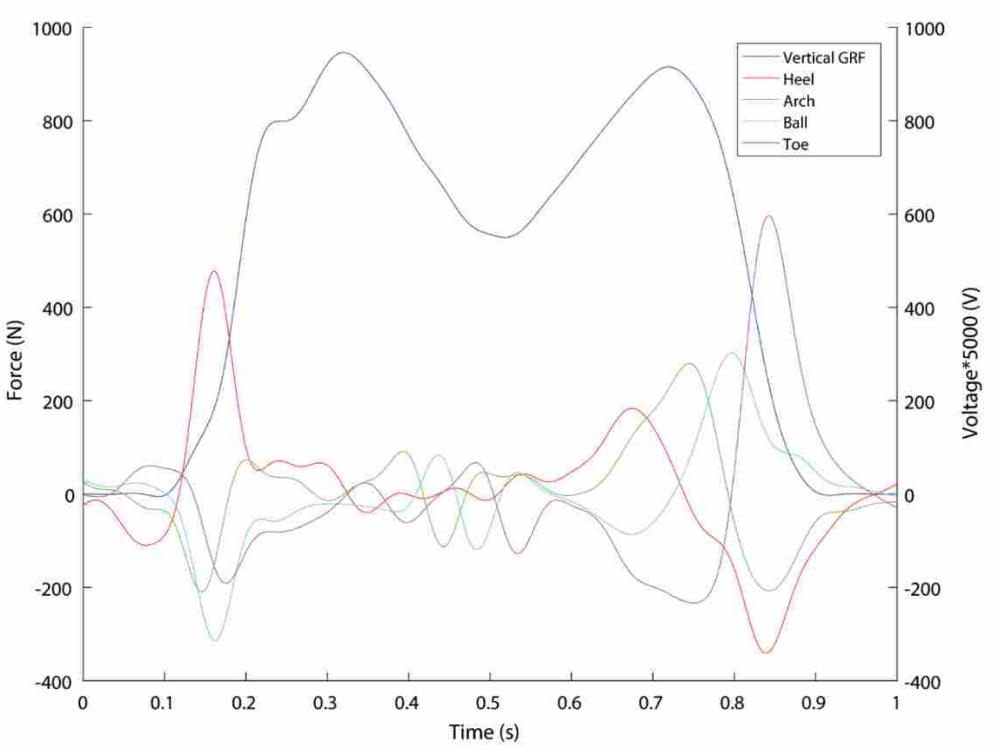


**Figure 3-3: A vertical ground reaction force (VGRF) curve for a single stance phase, time normalized to stance duration (horizontal axis), with corresponding signals from each sensor (heel, arch, ball and toe). Each sensor signal was scaled by 5000 to match the VGRF magnitudes.**

### 3.4 Results

Using cross validation to evaluate the selected SS model for each subject, the average error for the 3D GRF in the anterior-posterior, mediolateral, and vertical directions were 6.52 N (1.99%), 4.79 N (6.44%), and 15.4 N (2.08%), respectively. The average number K of amplitudes needed for models of the anterior-posterior, mediolateral, and vertical GRF were 22, 19, and 18, respectively. Mean Absolute Percent Error (MAPE) is reported along with MAE in order to normalize the results across subjects. To give an idea of how much absolute error varies from prediction to prediction, the Standard Deviation of the Absolute Error (SDAE) is also shown for each subject. These results for each subject can be found in APPENDIX A, Table A-I; whereas, the mean intra-subject results across all SS models can be seen in Figure 3-5.

Graphical examples of individual stance phases, one randomly selected stance phase, and the corresponding prediction of that stance phase from the SS model, for each GRF component, for one representative male and one representative female subject can be seen in Figure 3-4 (Similar graphics for each subject are shown in APPENDIX A).

The graphical results from each subject showed a larger variance between stances for mediolateral forces when compared to anterior-posterior and vertical forces. The vertical and anterior-posterior forces held the same shape across all subjects, whereas the mediolateral forces produced a unique pattern for each individual subject.

The CSV model was evaluated in two ways. First, a ten-fold cross validation analysis on all data combined was performed. The average MAE for GRF predictions in this case were 8.15 N (2.51%), 6.62 N (8.59%), and 19.3 N (2.60%) for the anterior-posterior, mediolateral, and vertical GRF models, respectively. Then another cross validation analysis on the data was performed, treating each subject, in turn, as the “test subject”. Average MAE for predictions in

this analysis were 29.0 N (9.11%), 37.0 N (46%), and 75.5 N (10.01%) for the anterior-posterior, mediolateral, and vertical GRF, respectively. For the CSV model, the number of amplitudes (K) used for the anterior-posterior, mediolateral, and vertical GRF models were 66, 66, and 78, respectively. CSV model accuracy for each "test subject", from cross-validation, can be found in APPENDIX A, Table A-II; whereas, the accuracy of mean inter-subject and intra-subject estimates, from cross-validation, can be seen in Figure 3-5.

Finally, a variable selection process (described in the previous section) was performed to determine which subject demographics should be included in the CSVD model. For anterior-posterior and vertical GRF, it was discovered that using only the weight of the subject yielded the model with the best predictive ability; however for mediolateral GRF, the best model was the one that included both the gender and height of the individual. After going through this variable selection process, the CSVD model was evaluated in the same way as the CSV model: first performing ten-fold cross validation on all data combined, and then removing "test subject" data for each subject in turn. The former analysis resulted in an average MAE of 7.64 N (2.35%), 5.35 N (7.05%), and 16.6 N (2.2%) for the anterior-posterior, mediolateral, and vertical GRF models, respectively. These average errors were lower than the resulting errors from the CSV model; confidence intervals around the average MAE were approximately zero implying that the difference in error is significant. The "test subject" cross validation gave an average MAE of 40.7 N (12.62%), 32.1 N (42.10%), and 64.8 N (7.42%) for anterior-posterior, mediolateral, and vertical GRF, respectively – these errors were again lower than errors from the CSV model, except in the case of anterior-posterior GRF. For the CSVD model, the number of amplitudes (K) were again 66, 66, and 78 for the anterior-posterior, mediolateral, and vertical GRF models, respectively. CSVD model accuracy for each "test subject", from cross-validation (including

subject demographic variables), can be found in APPENDIX A, Table A-III; whereas, the accuracy of mean inter-subject and intra-subject estimates, from cross-validation, can be seen in Figure 3-5.

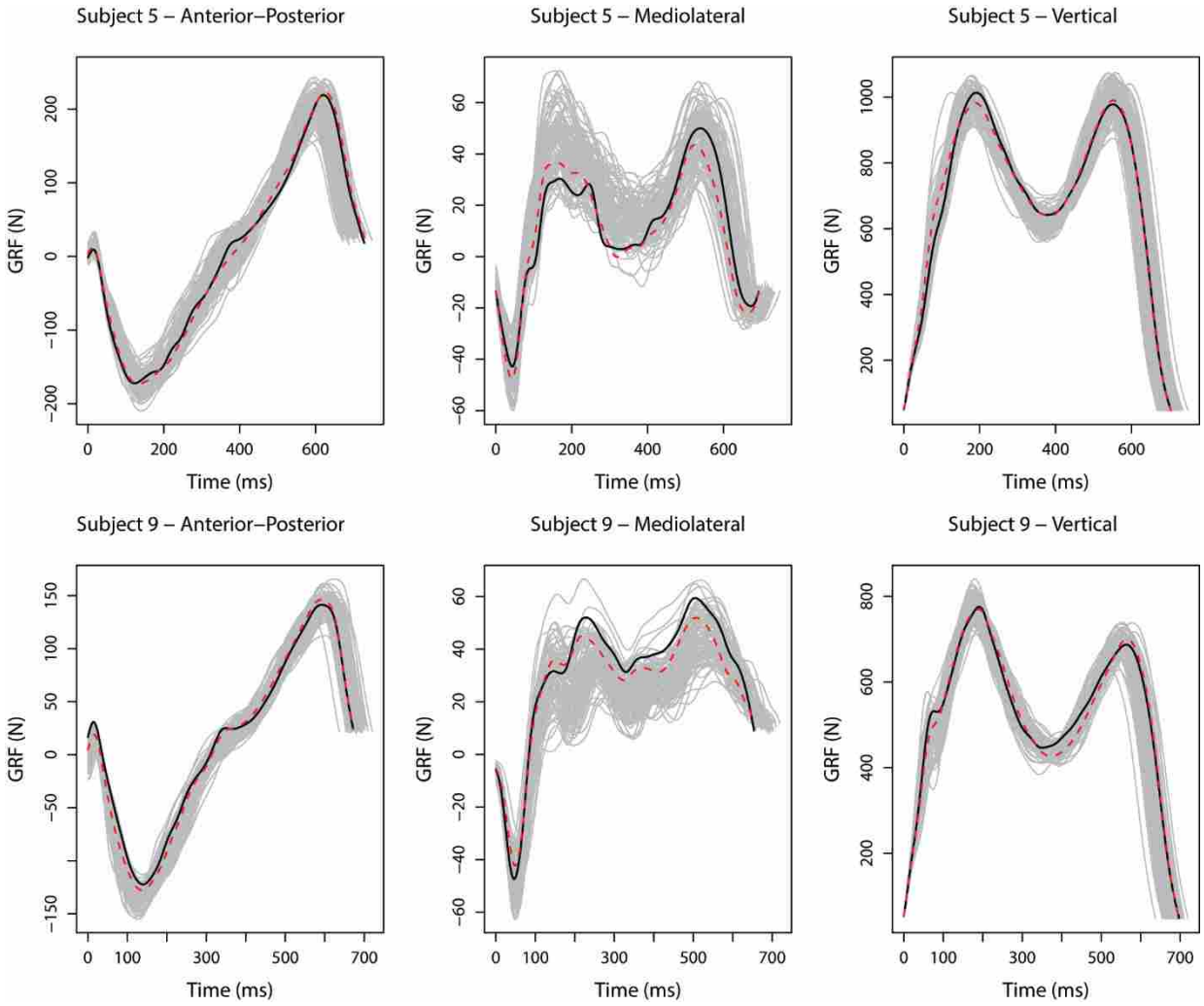


**Figure 3-4: Graphs of 3D GRF for one representative male (subject 5) and one representative female (subject 9) where the light grey lines represent each individual stance, the solid black line represents one randomly selected actual stance, and the dotted line represents the predicted curve from the Single Subject GRF model corresponding to the actual stance (black line).**

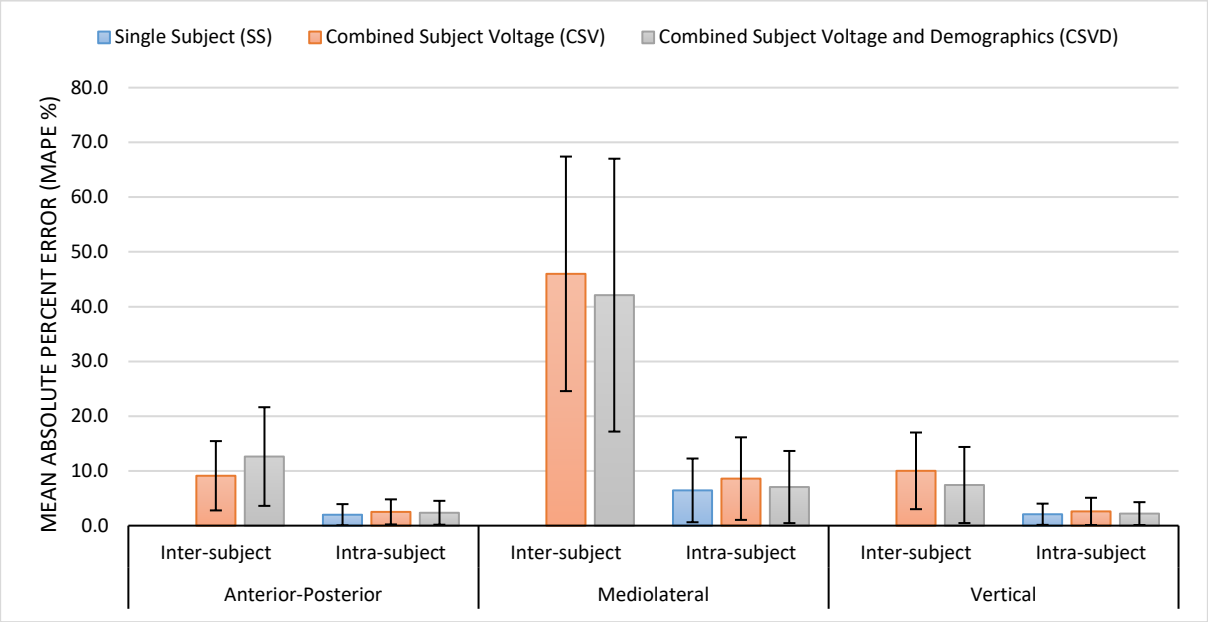


**Figure 3-5: A graph showing the mean absolute percent error (MAPE) of each statistical model used to estimate 3D ground reaction force (GRF). Three statistical models were tested: a model for each individual subject (SS) using nanocomposite piezoresponsive foam (NCPF) voltage data, a model using NCPF voltage data from all subject's combined (CSV), and a model using NCPF voltage data and demographic data from all subject's combined (CSVD). The SS, CSV, and CSVD models used all subject data to predict 3D GRF from within those subjects (intra-subject), where the mean error and standard deviation across all subjects were reported. The CSV and CSVD models were used to predict each subject separately (inter-subject), where the mean error and standard deviation across all "test subjects" were reported. All errors and standard deviations are calculated from cross-validation.**

## 3.5 Discussion

The present results demonstrate that our novel approach (NCPF sensors, inserted into the insole of an athletic shoe) can reasonably estimate 3D GRF during walking. For each of the nine subjects, a model was calibrated to the subject's 3D GRF and then used to estimate 3D walking GRF in a reasonably accurate manner. Additional models were created using 3D GRF from all subjects combined; these models were also able to estimate 3D walking GRF with comparable accuracy. The results showed that adding demographic variables to the combined-subject model

significantly decreased the error for in-sample predictions when compared to a model that only used NCPF sensor output. The generalized predictive ability of these models was tested on each subject when withheld from the calibration data set. Again, the results showed that adding demographic variables decreased the error for out-of-sample subject predictions, except in the case of anterior-posterior GRF where the error actually increased. This increased error was unexpected and might imply that anterior-posterior GRF may not be significantly related to subject demographics, although additional subject testing is required to validate this hypothesis. Results from these "test subject" estimates also showed a significantly higher average error when compared to the single subject model estimates. Although these inter-subject estimates had a higher error than the intra-subject estimates, we anticipate that with a larger sample of subjects a single, more comprehensive predictive model relating the sensor output with 3D GRF could be developed for the general population during walking.

As has been previously observed [70, 71], the mediolateral GRF exhibited greater stance-to-stance variability, relative to the anterior-posterior and vertical GRF. We suppose that this variability may have influenced the accuracy, of the corresponding sensor model, however, further testing must be carried out to evaluate this idea. The instrumented shoe contained four sensors placed along the anterior-posterior axis. This chosen distribution of sensors promotes accurate estimations with the least complexity; however, it may not be sufficient to accurately capture mediolateral forces because these forces act perpendicular to the line of sensors in the shoe. Thus, we also plan to study the influence of shoe sensor arrangement on the accuracy of 3D GRF estimation.

The accuracy of the estimated GRF for all three directions has shown to be comparable, if not greater, than other force sensing systems. From the SS models, the NCPF sensors were able

to estimate 3D GRF with an average error that ranged from 2% to 7% (MAPE), across all subjects; this is comparable to results obtained from the pneumatic bladder system used by Jacobs, et al. who reported errors of <10% for 3D GRF estimates [43]. The NCPF sensors showed an improved accuracy in estimating vertical GRF when compared to insoles instrumented with force sensing resistors where errors >5% were previously reported [44, 45]. NCPF sensor estimates of anterior-posterior and mediolateral GRF showed a large reduction in error when compared to results reported by Khurelbaatar et al., who used the Pedar-X® (Novel GmbH, Munich, Germany) commercial system [39]. The accuracy of our GRF estimates was comparable to results reported by Liu, et al. and Faber, et al., who used portable force plates [49, 66] and motion capture (kinematic) data [52], respectively. These previous studies reported errors between 1-7%; however, their cost, complexity, and attachment to the subject inhibit use in a natural environment; thus, NCPF sensors may be the preferred system of choice for data collection.

An advantage of the current implementation is that the model's accuracy has been shown for all three components of GRF, as seen in Figure 3-4. Additionally, the requirement for bulky electronics has been eliminated, as the only electronics required are a single microprocessor (approximately 4.33 g), with minimal power requirements, which communicates directly with the user's smartphone at a fraction of the cost of commercially available GRF estimation techniques. Furthermore, NCPF sensors can be embedded into the foam sole of a shoe with minimal interference to its feel and weight, which is an ideal criterion in wearable sensors [55].

There are some limitations to this study. Although this is an important preliminary exploration of a new technology, the present results describe a relatively small data set: nine subjects, walking at one speed, for a short amount of time. Because of the relatively small data

set, the generalizing capabilities of this method cannot yet produce 3D GRF estimates suitable for gait analysis applications unless a model is calibrated to each individual subject. To develop a more general predictive model across subjects, it will be necessary to evaluate data from a larger, more variable sample of subjects (i.e., different genders, ages, masses, etc.), ambulation speeds, including running, and conditions (e.g., graded surfaces). The NCPF revealed a signal drift that might be due to time and temperature that prevented data collection over long durations, commonly seen in real-life scenarios. To allow for longer test durations, the signal drift should be fully characterized so that any drift exhibited during testing can be fully corrected (e.g. using temperature sensors embedded in the shoe to account for any drift due to changes in temperature). Finally, the synchronization of sensors to force plates was based on an event (abruptly striking the right heel on the force platform) since each device was connected to a separate internal clock; this approach for data alignment may have introduced a slight horizontal shift in data over time.

In summary, we are able to estimate 3D GRF during walking using novel NCPF sensors. Nine subjects were tested, walking at one constant speed, and statistical models were produced that accurately estimated 3D GRF across the entire stance phase of gait. Two different approaches (data from each individual subject and data from all subjects) resulted in 3D GRF estimates that ranged in average MAE from 6 N (anterior-posterior GRF) to 20 N (vertical GRF) for intra-subject GRF measurements and from 28 N (anterior-posterior GRF) to 64 N (vertical GRF) for inter-subject GRF measurements. The intra-subject models produced acceptable levels of accuracy, while inter-subject models will require additional work to provide improved accuracy, primarily the collection of a much larger body of subject data to serve as the basis for the model. Also, future work will include testing subjects as they perform other activities (e.g.,

running, jumping, landing), to determine how useful these sensors are in estimating general motion. We also plan to collect walking data on more subjects, to improve our model estimates. We anticipate that with continued data collection, across a larger, more heterogeneous sample of subjects, we will be able to estimate 3D GRF with more accuracy. NCPF sensors might be a viable alternative to traditional force plates and have potential to be used as mobile sensors to accurately estimate 3D GRF during human walking, outside of the traditional laboratory environment.

# 4 MODELING GROUND REACTION FORCE USING ARTIFICIAL NEURAL NETWORKS

## 4.1 Abstract

Previous work has shown that statistical modeling can provide accurate predictions of 3D ground reaction force (GRF) using input data from nanocomposite piezoresponsive foam (NCPF) sensors. Although the results from these models have proven accurate, the predictive capabilities have not been validated. An alternative approach using artificial neural networks (ANN) may be able to provide better predictive estimates while maintaining comparable accuracy. Nine subjects (5 male, 4 female) walked on a force-instrumented treadmill at 1.34 m/s (3 mph) for 120 s each while wearing a shoe that was instrumented with four NCPF sensors. GRF data, measured by the treadmill, and sensor data, measured by the NCPF sensors, were used in a three-layer artificial neural network (ANN) to calibrate a separate model for each individual. The calibrated models estimated average anterior-posterior, mediolateral and vertical GRF with an average error of 7.46 N (3.66%), 5.07 N (11.17%), and 14.62 N (0.98%), respectively. Using all subject data combined, calibrated models estimated average anterior-posterior, mediolateral and vertical GRF with an average error of 9.86 N (4.43%), 8.14 N (22.48%), and 22.18 N (1.70%), respectively. To test the predictive capabilities of an ANN model, a single subject was recruited to perform a calibration protocol while wearing an NCPF instrumented shoe. The subject ran on a force-instrumented treadmill at seven different speeds (2, 3, 4, 5, 6, 7, and 8

mph) for 30 s each while wearing an NCPF instrumented shoe; this data set was used to train two kinds of ANN models: one for predicting vertical GRF (VGRF) curves, and the other for predicting VGRF characteristics. The subject then ran at three randomly selected speeds from within the calibration range (3, 6.5, and 8 mph) for 30 s each; this data set was used to test both VGRF models. After calibration, the model estimated test VGRF curves with an average error of 48.40 N (3.73%). The other model estimated peak impact force (PIF), time to peak impact force (TPIF), and stance duration (SD) from test VGRF data with an average error of 61.05 N (5.37%), 7.20 ms (8.32%), and 23.49 ms (4.12%), respectively. The predictive capabilities of an ANN model for estimating GRF within a subject across a range of speeds has been validated opening new possibilities for mobile GRF collection.

## 4.2 Introduction

Kinetic measurements are an essential element for performing gait analysis. Kinetic data are required to determine reaction forces and torques across various joints of the body [25]. Standard methods for collecting kinetic information involve having a subject walk across a static force plate (usually embedded in the ground) to collect several stance phases for analysis. These force plates are able to collect three dimensional (3D) ground reaction force (GRF) data and center of pressure (COP) data with a high degree of accuracy; however, their lack of mobility and expensive costs prohibit large data collection and analysis outside of a clinical setting [35].

To collect 3D GRF data outside of a laboratory environment, wearable sensors and other force transducing devices have been developed and tested. Pressure transducing sensors have been used in several custom-made insoles to detect GRF and COP [44]. Other pressure sensors such as pneumatic air bladders [43], force sensing resistors [45], and mobile tri-axial force plates [49] have also been tested to measure GRF in a mobile setting. Although these developments

have shown promising results, the cost [43], size and weight [49], and accuracy of their estimations [44] could still be improved.

Recently developed nanocomposite piezoresponsive foam (NCPF) sensors may be a viable alternative to current wearable sensors for accurately measuring 3D GRF without inhibiting the user's natural gait. Previous research has shown that carbon-based nanoparticles can enhance the electrical properties of flexible materials [60]. This enabled the creation of high deflection strain gauges made from silicone, which were able to detect strain as high as 60% [58]. It was observed that by adding nickel-coated nanoparticles to a polyurethane foam matrix, a voltage potential is created when the foam is impacted [61]. The resulting NCPF sensors have been used as bushings for a planetary centrifuge to determine frequency output [62]. This unique ability for the material to fulfill both a mechanical and sensor role makes them desirable by users as a wearable sensor, because of their low weight, complexity, and embedded capabilities [55].

Previous work has shown that NCPF sensors can estimate walking 3D GRF with comparable accuracy to current wearable sensors [72]. In that study, a statistical approach was used to develop a model for predicting walking GRF; however, predictive capabilities for this model were not fully examined (e.g. GRF estimates for other speeds outside of walking). Machine learning algorithms such as artificial neural networks (ANN) have been used for developing complex, non-linear models with predictive capabilities [65]. This method has been used to predict GRF using three tri-axial force plate data with a high degree of accuracy [53]. It is anticipated that a similar ANN model can be created for predicting GRF across a range of running speeds using NCPF sensor data. This paper presents the testing and validation of an ANN modeling approach for estimating 3D GRF.

## 4.3 Estimating Walking 3D Ground Reaction Force (GRF)

### 4.3.1 Materials and Methods

To compare the modeling capabilities between ANN and statistical methods used previously, an analysis was done on the same multi-subject walking data from the study performed by Rosquist et al. [72]. In this study, nine subjects (5 male, 4 female) were recruited to walk at 1.34 m/s (3 mph) on a force-plate embedded treadmill (AMTI, Watertown, MA, USA) while wearing a shoe instrumented with four NCPF sensors under the insole (heel, arch, ball, and toe). Each subject walked at this constant speed for 120 s while force and sensor data were collected simultaneously. After collection, post-processing procedures were performed in MATLAB® (MathWorksTM, Natick, MA, USA). Data collected from the force plate, motion cameras, and microcontroller were sampled at 1000 Hz, 250 Hz, and 1029 Hz, respectively. Reflective markers attached at the heel, toe, and lateral positions of the shoe were used to create a model of a foot in Visual3D software (C-Motion Inc., MD, USA), in order to identify which force curves corresponded to the shoe with the NCPF sensors. Protocol for NCPF sensor development and data processing followed the same procedure outlined by Rosquist et al. [72].

To isolate force and sensor data for each individual stance phase, a data separation process was repeatedly followed. All force and sensor data were filtered using a fourth order Butterworth low pass filter with a cutoff frequency of 21 Hz. The filtered data (GRF and sensor) were separated into individual stance phases using a threshold of 50 N on the vertical GRF (VGRF) to identify heel strike and toeoff positions (heel strike was identified when the VGRF exceeded the threshold and toeoff was identified when the VGRF subsequently fell below the threshold). Following separation, force and sensor data for each stance phase were normalized to three hundred-fifty evenly spaced data points. Ten percent of the total stances collected for each

subject were randomly selected and removed to be a test data set for the ANN model. The remaining ninety percent of the stance phases were then used as a training data set to build an ANN model using MATLAB's Neural Network Toolbox [73].

A feedforward, three layer (input, hidden, and output) network was utilized to develop a non-linear regression model for estimating 3D GRF curves. The input layer contained 1400 nodes (350 data points for each of the 4 sensors per stance), the hidden layer contained 10 nodes, and the output layer contained 350 nodes (350 data points for one-direction of GRF). The network utilized a backward-propagation algorithm with the gradient steepest-descent method to update the weights for the nodes at each layer, and a sigmoid activation function was applied to the hidden layer nodes. The input data for the network consisted of an n x 1400 array of filtered sensor data points for each stance of the trial (350 x 4 = 1400, n = number of stances). The output data consisted of an n x 350 array of filtered GRF data points for each stance of the trial. To develop the model, 80% of the training data was used to train the network and the remaining 20% of the training data was used to validate the network.

To show the generalized capabilities of ANN models across subjects, 3D GRF models were also created using the entire subject data combined. Three cases of combined subject data were examined: all data, all female data, and all male data. Because two separate sensor systems were used (one system in the male shoe and another system in the female shoe), a question of interest was whether combining data from different sensor systems would still yield accurate GRF estimates. These combined subject data sets were again separated into training and testing data sets, where a randomly selected 10% of the stance phases were used as the test set and the remaining 90% were used as the training set. The accuracy of each subject-specific (SS) and combined-subject (CS) GRF model using the test data sets was reported using the Mean

Absolute Error (MAE) and the Mean Absolute Percent Error (MAPE). The MAE for each stance phase was calculated using Equation 4-1 and the MAPE for each stance phase was calculated using Equation 4-2,

$$MAE = \frac{1}{n}\sum_{i=1}^{n}|f_i - y_i| \tag{4-1}$$

$$MAPE = \frac{100}{n}\sum_{i=1}^{n}\left|\frac{y_i - f_i}{y_i}\right| \tag{4-2}$$

where $n$ is the total number of data points in a stance phase, $f_i$ is the estimated data point, and $y_i$ is the actual data point. The mean MAE, standard deviation of the MAE (SDAE), and mean MAPE across all stance phases were calculated and reported as the average errors for that model.

### 4.3.2 Results

The SS models estimated GRF along the anterior-posterior, mediolateral, and vertical axis with a MAE of 7.46 N (3.66%), 5.07 N (11.17%), and 14.62 N (0.98%), respectively. Table 4-I summarizes the results of each subject model for each axis of GRF. A graphical example of each GRF model for one representative male and one representative female is shown in Figure 4-1. Similar graphics for each subject can be found in APPENDIX B.

The CS model using all male data estimated GRF along the anterior-posterior, mediolateral, and vertical axis with a MAE of 11.81 N (5.54%), 8.15 N (17.81%), and 22.69 N (1.59%), respectively. The CS model using all female data estimated GRF along the anterior-posterior, mediolateral, and vertical axis with a MAE of 7.98 N (4.35%), 6.86 N (18.23%), and 18.14 N (1.73%), respectively. The CS model using all subject data estimated GRF along the anterior-posterior, mediolateral, and vertical axis with a MAE of 9.86 N (4.43%), 8.14 N (22.48%), and 22.18 N (1.70%), respectively. Table 4-II summarizes the results of the CS models for each axis of GRF. A graphical example of each CS model is shown in Figure 4-2, Figure 4-3, and Figure 4-4.

**Table 4-I: Reported absolute error (MAE), absolute percent error (MAPE), and standard deviation of absolute error (SDAE) of the artificial neural network (ANN) model for each subject, along with averages across all subjects, for each GRF direction.**

| | | | | | Anterior-Posterior | | | Mediolateral | | | Vertical | | |
|---|---|---|---|---|---|---|---|---|---|---|---|---|---|
| **Subject** | **Sex** | **Age (yrs)** | **Height (cm)** | **Mass (kg)** | **MAE (N)** | **MAPE (%)** | **SDAE (N)** | **MAE (N)** | **MAPE (%)** | **SDAE (N)** | **MAE (N)** | **MAPE (%)** | **SDAE (N)** |
| **1** | F | 25 | 167.6 | 59.0 | 5.29 | 3.69 | 1.60 | 5.17 | 11.83 | 2.09 | 12.19 | 1.06 | 4.19 |
| **2** | M | 26 | 172.7 | 79.8 | 6.98 | 4.39 | 2.14 | 4.72 | 11.97 | 2.39 | 15.87 | 1.13 | 4.84 |
| **3** | F | 21 | 172.7 | 56.7 | 9.67 | 5.35 | 3.34 | 6.67 | 13.50 | 2.21 | 13.08 | 0.79 | 5.28 |
| **4** | M | 27 | 185.4 | 68.0 | 8.49 | 2.96 | 3.12 | 5.05 | 6.53 | 1.57 | 13.72 | 0.83 | 4.01 |
| **5** | M | 23 | 169.5 | 85.3 | 9.30 | 4.35 | 2.87 | 5.56 | 11.61 | 2.26 | 21.32 | 1.14 | 7.32 |
| **6** | M | 23 | 172.7 | 65.8 | 10.37 | 3.96 | 3.57 | 5.01 | 12.88 | 1.69 | 18.33 | 1.43 | 6.25 |
| **7** | M | 22 | 170.2 | 76.2 | 6.17 | 2.68 | 2.20 | 4.97 | 10.18 | 2.20 | 13.41 | 0.88 | 4.38 |
| **8** | F | 24 | 157.5 | 53.5 | 5.46 | 2.43 | 1.64 | 3.85 | 11.58 | 1.73 | 8.48 | 0.68 | 2.42 |
| **9** | F | 24 | 172.0 | 62.0 | 5.44 | 3.15 | 1.68 | 4.67 | 10.48 | 1.95 | 15.19 | 0.88 | 4.86 |
| **Average** | - | 24 | 171.2 | 67.4 | **7.46** | **3.66** | **2.46** | **5.07** | **11.17** | **2.01** | **14.62** | **0.98** | **4.84** |

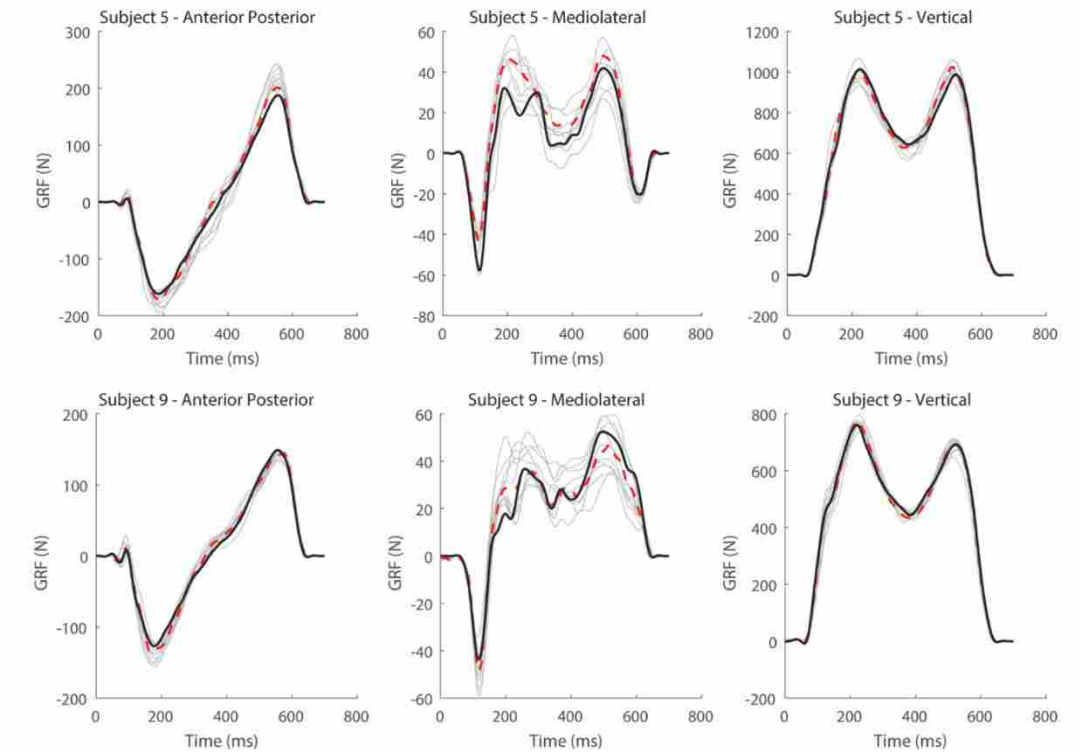


**Figure 4-1: Graphs of 3D ground reaction force (GRF) for one representative male (subject 5) and one representative female (subject 9), where the grey lines represent GRF curves for each test stance phase, the solid black line represents one randomly selected actual GRF curve, and the dotted red line represents the predicted GRF curve corresponding to the actual GRF curve.**

**Table 4-II: Reported absolute error (MAE), absolute percent error (MAPE), and standard deviation of absolute error (SDAE) of the artificial neural network (ANN) model for each combined-subject data set.**

| | Anterior-Posterior | | | Mediolateral | | | Vertical | | |
|---|---|---|---|---|---|---|---|---|---|
| **Data Set** | **MAE (N)** | **MAPE (%)** | **SDAE (N)** | **MAE (N)** | **MAPE (%)** | **SDAE (N)** | **MAE (N)** | **MAPE (%)** | **SDAE (N)** |
| **Male** | 11.81 | 5.54 | 2.84 | 8.15 | 17.81 | 2.22 | 22.69 | 1.59 | 6.95 |
| **Female** | 7.98 | 4.35 | 2.85 | 6.86 | 18.23 | 2.68 | 18.14 | 1.73 | 5.49 |
| **All** | **9.86** | **4.43** | **3.69** | **8.14** | **22.48** | **2.59** | **22.18** | **1.70** | **6.66** |

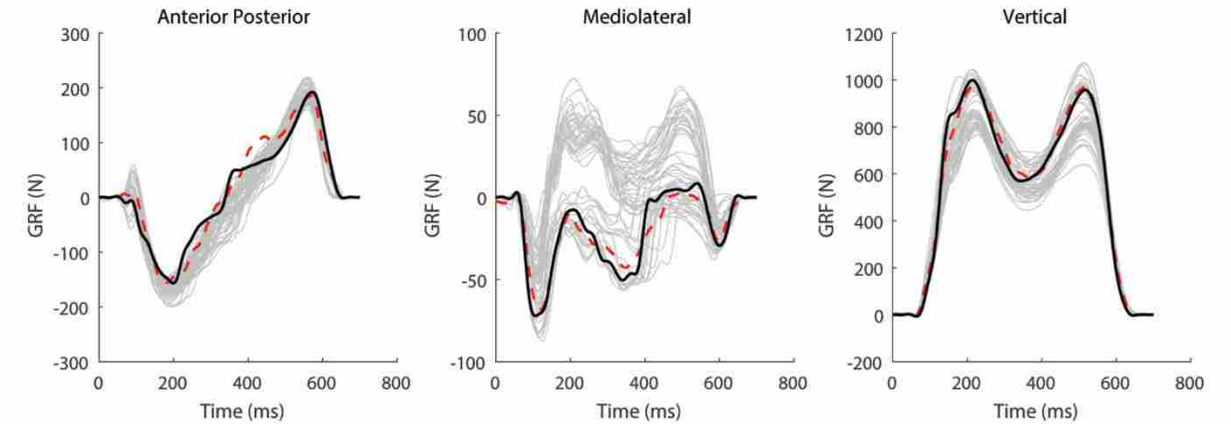


**Figure 4-2: Graphs of 3D ground reaction force (GRF) from the ANN models that used all male subject data combined, where the grey lines represent GRF curves for each test stance phase, the solid black line represents one randomly selected actual GRF curve, and the dotted red line represents the predicted GRF curve corresponding to the actual GRF curve.**

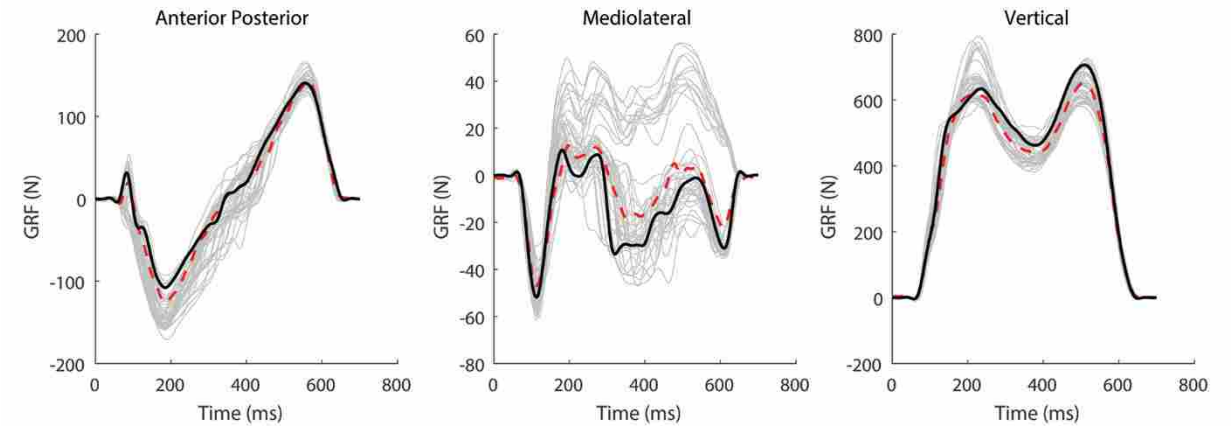


**Figure 4-3: Graphs of 3D ground reaction force (GRF) from the ANN models that used all female subject data combined, where the grey lines represent GRF curves for each test stance phase, the solid black line represents one randomly selected actual GRF curve, and the dotted red line represents the predicted GRF curve corresponding to the actual GRF curve.**

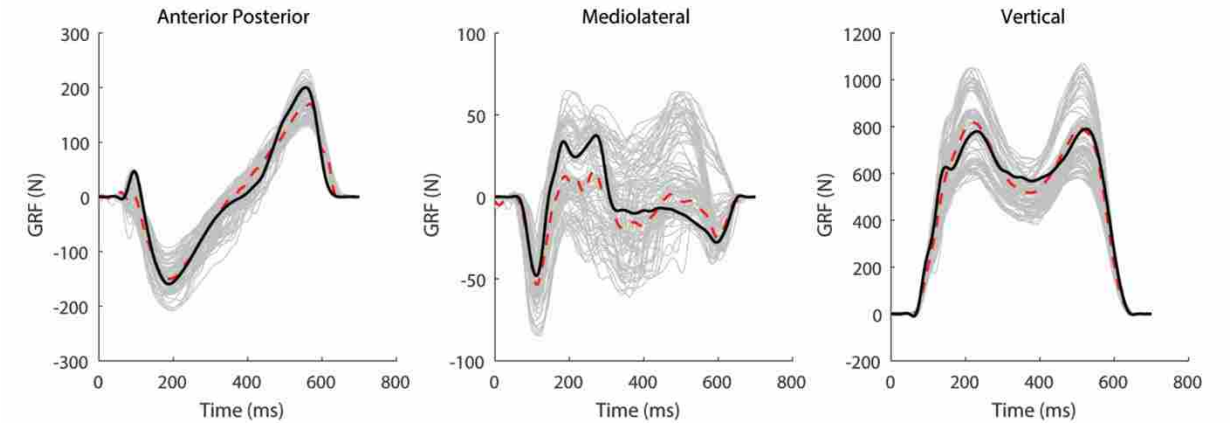


**Figure 4-4: Graphs of 3D ground reaction force (GRF) from the ANN models that used all subject data combined, where the grey lines represent GRF curves for each test stance phase, the solid black line represents one randomly selected actual GRF curve, and the dotted red line represents the predicted GRF curve corresponding to the actual GRF curve.**

## 4.4 Estimating Vertical Ground Reaction Force (VGRF) Curves and Characteristics

### 4.4.1 Materials and Methods

When estimating 3D GRF using an ANN model, it was found that estimates across subjects was most accurate for vertical GRF (VGRF). To understand the predictive capabilities of ANN models, it was desired to test whether a subject-specific ANN model could predict VGRF curves and characteristics across a range of gait speeds. A pilot subject (age, 25 years; height, 171.45 cm; mass, 59.87 kg; shoe size, US Men's 9.5) volunteered to perform two separate running trials: calibration and testing. This subject was recruited and followed protocol approved by the university institutional review board.

The subject performed a calibration test by running on the aforementioned force-sensing treadmill while wearing an NCPF instrumented shoe on the right foot. This test consisted of having the subject run for 30 s increments at seven different speeds (2, 3, 4, 5, 6, 7, and 8 mph)

in a randomized order. Following the calibration period, the subject then ran for 30 s increments at three different speeds in a randomized order (3, 6.5, and 8 mph), which would be used to test the calibration model's accuracy. This test data set would provide a walking, running, and unknown speed through which the generalization of an ANN model could be shown. All subject protocol and data processing procedures used in the aforementioned multi-subject walking study were also used in this pilot study.

Two kinds of VGRF data were of interest in this pilot study: the VGRF curve, and specific VGRF characteristics. From the VGRF curve, characteristics such as peak force [29, 30], loading rate [31], and stance time [74] have been found to be important indicators of lower limb stress fractures and running performance. The peak impact force (PIF), time to peak impact force (TPIF), and stance duration (SD) were chosen as variables of interest for an ANN model to see if these characteristics could be directly predicted rather than calculated from an estimated curve.

To estimate the VGRF curve, the same MATLAB ANN was used from the multi-subject walking study; however, to prevent the model from overfitting the calibration data, three nodes were used in the hidden layer instead of ten. This approach worked when estimating a single output data type (e.g. force); however, it failed to accurately train a model when multiple outputs with different magnitudes and units were desired (e.g. force and time). To simultaneously estimate each VGRF characteristic using a single model, the Visual Gene Developer (VGD) neural network toolbox [75] was selected over the MATLAB Neural Network Toolbox. The VGD neural network consisted of a feedforward three-layer network with ten nodes in the hidden layer and used a hyperbolic tangent transfer function. Input data to the network were an n x 24 matrix, where six variables were taken from each of the four sensors: maximum voltage,

minimum voltage, absolute integral, maximum voltage rate, time to maximum voltage, and time to minimum voltage (6 x 4 = 24 variables, n = number of stances). Output data for the network were an n x 3 matrix, where the three VGRF variables were PIF, TPIF, and SD. Both input data and output data were normalized to be between -1 and 1 by dividing each variable by its maximum value from within the data set. Ninety percent of the calibration data was used to train the model over 10,000 iterations and the other ten percent was used to validate the model. After training the model, all data was multiplied by the normalizing factor to show the estimates on their original scale.

After training and validation, test data were put through the model and the accuracy of those estimates were validated via statistical measures. To measure the accuracy of the VGRF curve the same statistical measures (MAE, MAPE, and SDAE) were calculated and reported as was for the multi-subject walking study. To measure the accuracy of the VGRF characteristics model, the MAE, MAPE, and Pearson correlation coefficient (r) were calculated and reported.

### 4.4.2 Results

Using an ANN model developed in MATLAB from the calibration data, estimated VGRF curves had an average MAE of 48.40 N, a SDAE of 19.34 N, and an average MAPE of 3.73%. These results are summarized in Table 4-III. Graphs of a randomly selected stance phase with its corresponding estimate for the 3, 6.5, and 8 mph test data can be seen in Figure 4-5, Figure 4-6, and Figure 4-7.

**Table 4-III: Reported absolute error (MAE), absolute percent error (MAPE), and standard deviation of absolute error (SDAE) from the artificial neural network (ANN) model for the test data set curves.**

| | MAE (N) | MAPE (%) | SDAE (N) |
|---|---|---|---|
| **Test Curves** | 48.40 | 3.73 | 19.34 |

Using an ANN model developed in VGD from the calibration data, estimated PIF, TPIF, and SD had a MAE of 61.05 N (5.37%), 7.20 ms (8.32%), and 23.49 ms (4.12%), and r of 0.97, 0.93, and 0.99, respectively. These results are summarized in Table 4-IV. A plot of the actual value versus the estimated value for each VGRF characteristic, with their corresponding goodness of fit ($R^2$) value, can be seen in Figure 4-8, Figure 4-9, and Figure 4-10.

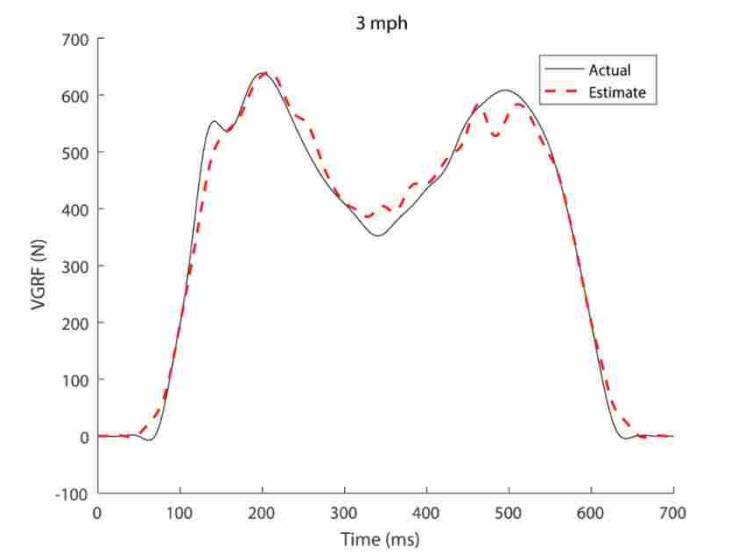


**Figure 4-5: One randomly selected stance phase of actual (black solid line) and estimated (red dotted line) vertical ground reaction force (VGRF) curves when the subject walked at 3 mph.**

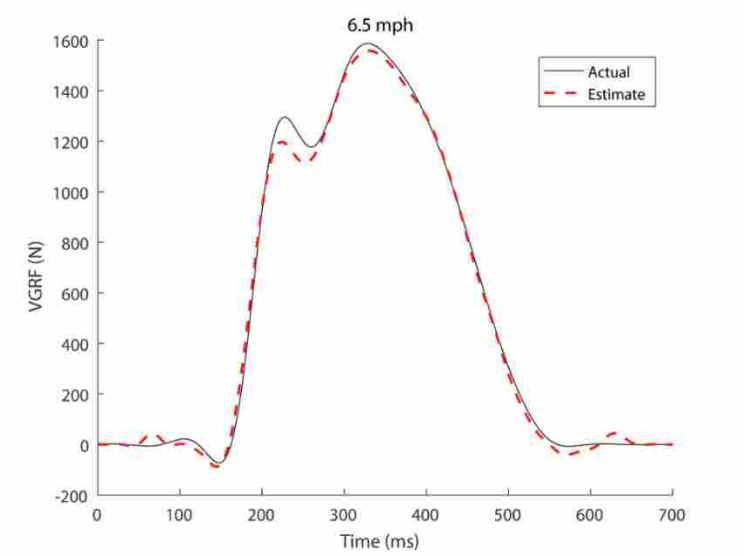


**Figure 4-6: One randomly selected stance phase of actual (black solid line) and estimated (red dotted line) vertical ground reaction force (VGRF) curves when the subject walked at 6.5 mph.**

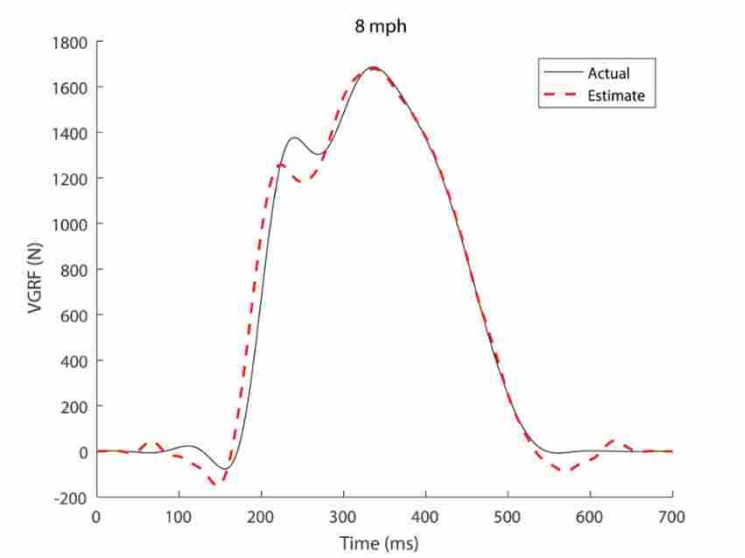


**Figure 4-7: One randomly selected stance phase of actual (black solid line) and estimated (red dotted line) vertical ground reaction force (VGRF) curves when the subject walked at 8 mph.**

**Table 4-IV: Reported absolute error (MAE), absolute percent error (MAPE), and Pearson correlation coefficient (r) from the artificial neural network (ANN) model for the test data set characteristics.**

| | MAE | MAPE | r |
|---|---|---|---|
| **Peak Impact Force** | 61.05 N | 5.37 % | 0.97 |
| **Time to Peak Impact Force** | 7.20 ms | 8.32 % | 0.93 |
| **Stance Duration** | 23.49 ms | 4.12 % | 0.99 |

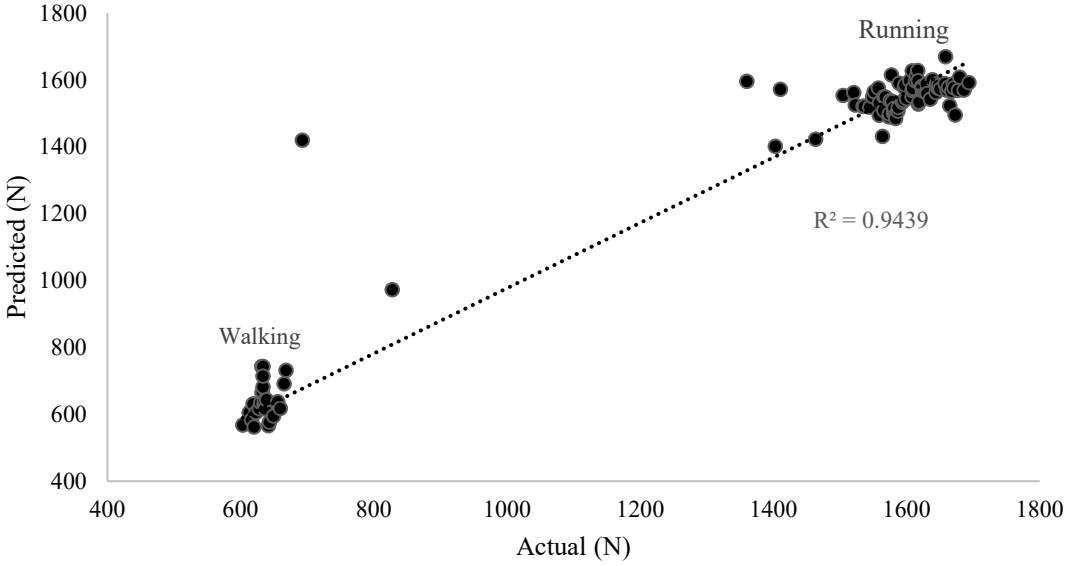


**Figure 4-8: A plot of the actual peak impact force (PIF) vs the predicted PIF for the test data set. The coefficient of determination quantifying the model's goodness of fit is shown below the trendline.**

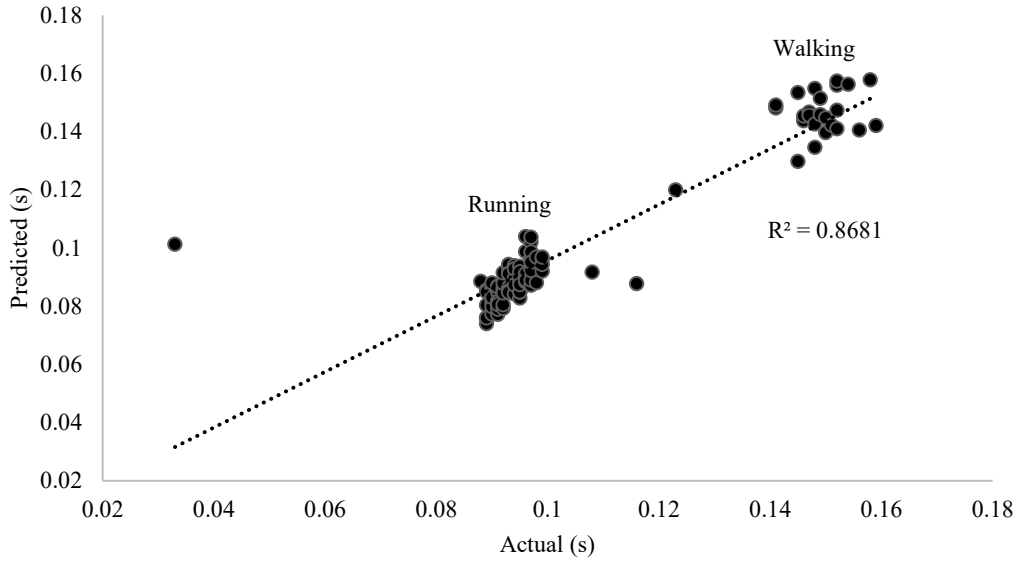


**Figure 4-9: A plot of the actual time to peak impact force (TPIF) vs the predicted TPIF for the test data set. The coefficient of determination quantifying the model's goodness of fit is shown below the trendline.**

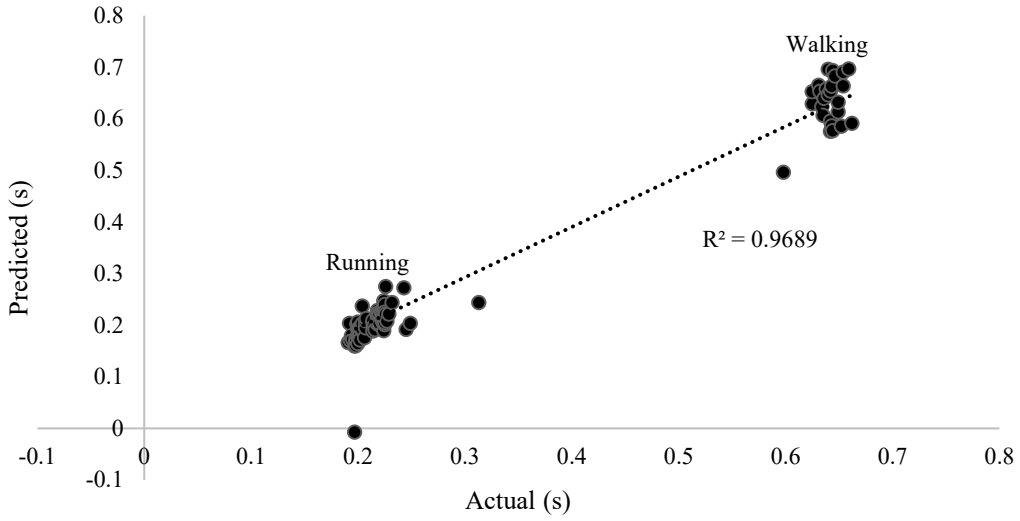


**Figure 4-10: A plot of the actual stance duration (SD) vs the predicted SD for the test data set. The coefficient of determination quantifying the model's goodness of fit is shown below the trendline.**

## 4.5 Discussion

The ability to estimate 3D GRF using NPCF sensors has been validated by implementing an ANN modeling approach. Subject-specific models were developed for nine different subjects to estimate 3D GRF during walking. The results from these models showed comparable accuracy to results from statistical models performed in previous research. The ability for an ANN model to predict unknown GRF has also been shown via the single-subject pilot study. After performing a brief calibration, the subject performed a separate test running at three different speeds; two of these speeds were performed during calibration, whereas the other speed was unknown to the model. The results showed that the ANN models were able to estimate VGRF curves and characteristics for these test speeds with relatively low error. The ability to accurately predict 3D GRF and VGRF within a range of exercises is an essential step towards performing gait analysis outside of a laboratory environment.

A comparison of the statistical modeling performed by Rosquist et al. [72] to ANN modeling shows that similar accuracy was obtained for 3D GRF estimates, except in the case of mediolateral GRF. Using SS data sets, the ANN model was able to estimate anterior-posterior GRF with an average error of 3.66%. This is comparable to the accuracy of the statistical model, which estimated anterior-posterior GRF with an average error of 1.99%. The ANN model estimated VGRF with an average error of 0.98%; this was an improvement from the statistical model, which estimated VGRF with an average error 2.08%. The largest discrepancy between the statistical and ANN models was the accuracy in measuring mediolateral GRF; the statistical model estimates had an average error of 6.44%, whereas the ANN model estimates had an average error of 11.17%. This same difference in results was also found in the CS data sets, where the statistical model estimated anterior-posterior, mediolateral, and vertical GRF with an

average error of 2.51, 8.59, and 2.60% respectively, and the ANN model estimated anterior-posterior, mediolateral, and vertical GRF with an average error 4.43, 22.48, and 1.70%, respectively. A visual comparison of the results from ANN and statistical models can be seen in Figure 4-11. Although errors were higher for the models using the CS data set with both male and female subjects combined, compared to the models using either male or female CS data sets separately, the same relative difference in error between vertical and mediolateral GRF was observed in both male and female CS data set models. The difference in accuracy between sensor systems (male vs female) when compared to using all data combined, suggests that ANN models should be produced for each individual sensor system to provide the most accurate estimates.

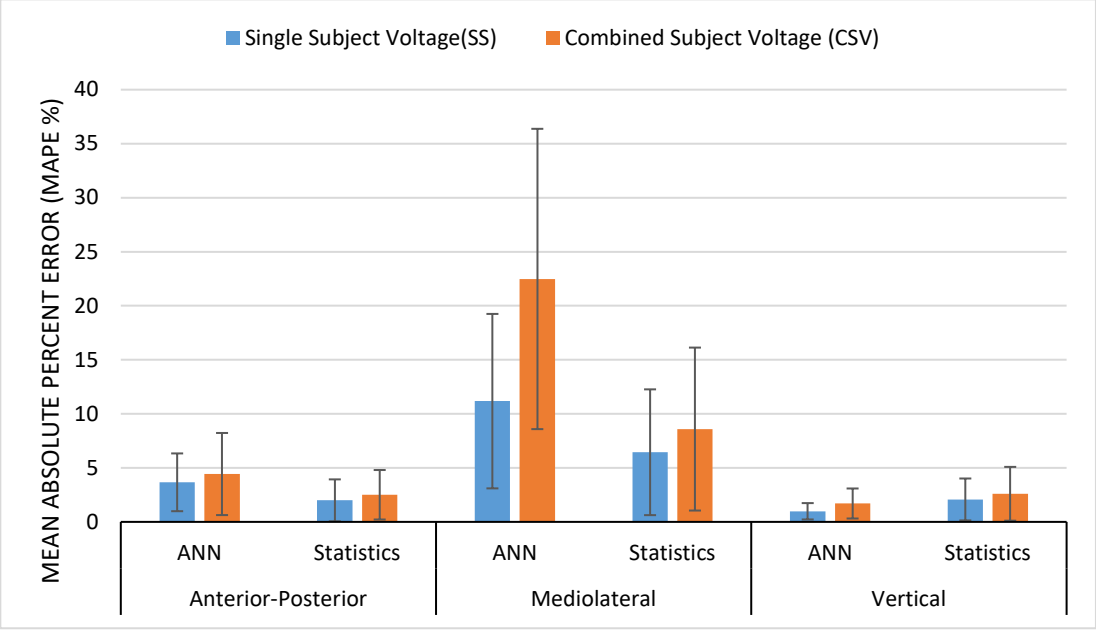


**Figure 4-11: A graph showing the mean absolute percent error (MAPE) of the artificial neural network (ANN) models and statistics models to estimate 3D ground reaction force (GRF). Two types of models were tested in each case: a model for each individual subject (SS) using nanocomposite piezoresponsive foam (NCPF) voltage data, and a model using NCPF voltage data from all subject's combined (CSV). The SS and CSV models used all subject data to predict 3D GRF from within those subjects (intra-subject), where the mean error and standard deviation across all subjects were reported.**

The difference in accuracy between ANN models and statistical models may also be explained by the variance between stances for VGRF and mediolateral GRF; the VGRF stances appeared to be very repeatable, whereas the mediolateral GRF stances had an extremely large variance. Because ANN modeling requires an extremely large amount of consistent training data to produce an accurate model, the number of stance phases for mediolateral GRF may not have been enough to train the model to account for the large variance between stances. This would also explain why the ANN model was able to estimate VGRF curves with higher accuracy when compared to the statistical model.

The ability to predict VGRF was also examined using a calibration/testing procedure, where an ANN model was trained using calibration data, and then tested using a separate data set that fit within the calibration range. A single subject calibrated a model by running at seven different speeds, after which, the model estimated VGRF curves for three different speeds found within that calibration range. Using this approach, the model estimated VGRF curves with an average error of less than 4%. In addition to estimating the entire curve, three different VGRF characteristics were also estimated via another ANN model. This model estimated PIF, TPIF, and SD with an average error of less than 5.40, 8.40, and 4.0%, respectively. These models produced VGRF estimates that were highly correlated to the actual values ($r > 0.90$). When comparing the estimated values to the actual values for each characteristic, two groupings of data appeared on the graphs. These distinct groupings can be related to speeds that result in either a walking or running gait. The model estimates for TPIF produced a significantly higher error than the other characteristic estimates. This increased error may be a result of inaccurate measurements of the PIF location, especially during speeds where the VGRF curve does not display a distinct dual stance shape (e.g. 4 mph walking). Stances performed when the treadmill

was either increasing or decreasing speed displayed an irregular shape, which may also explain the highly inaccurate estimates of certain VGRF characteristics (e.g. an estimated TPIF with a negative value). To create a more accurate model, it is recommended that all stances from transitioning speeds be removed from the input data set.

The purpose of these studies was to implement NCPF sensors in a shoe and validate that 3D GRF could be estimated using an ANN model. To validate this concept, models were trained using either single subject data, or all data combined, to predict GRF for subjects contained within the training data set. In addition, ANN models were developed to estimate VGRF at different speeds within a single subject. The results from these models showed that calibrating the model to each individual subject is an effective approach for accurately measuring 3D GRF, and that those subject-specific models are capable of predicting GRF across a range of gait speeds.

Although this initial proof of concept has been validated, there is still additional work that needs to be done to show the full capability of an ANN modeling approach. It is recommended that future studies be performed to examine the possibility of creating a single generalized model to predict 3D GRF across multiple subjects for a given range of gait speeds. This can be achieved by collecting data from a significantly larger sample size of subjects to try and encapsulate the general gait of the population. To test the repeatability and consistency of these sensors, it is also suggested that duplicate tests be performed on different days for each subject. By examining cross-subject, cross-speed predictions from a single ANN model, the robustness of NCPF sensors can be realized in real-world applications.

The present results indicate that ANN modeling is an effective approach for estimating 3D GRF; however, there are limitations to these studies that must be addressed. The duration of

measured gait used for training and testing was very short and does not represent realistic gait durations. To show that a calibration protocol was possible, a shorter time was selected; however, for future studies, it is recommended that longer periods of gait be collected. A longer testing duration may reveal signal drift and mechanical degradation that was not observed in these studies. These issues would need to be corrected to enable future out-of-lab applications. The accuracy of the intra-subject VGRF model was reported on data where the three test speeds were combined. To understand how accurately the model can estimate unknown speeds compared to calibration speeds, it is recommended that prediction errors be reported for each speed individually rather than collectively.

In conclusion, the ability to estimate 3D GRF from a system of NCPF sensors using an ANN has been validated, especially in the case of VGRF. Nine subjects were tested walking at 3 mph while wearing a shoe instrumented with NCPF sensors. From these tests, ANN models were created for each subject resulting in estimates of anterior-posterior, mediolateral, and vertical GRF with a MAE of 7.46 N (3.66%), 5.07 N (11.17%), and 14.62 N (0.98%), respectively. When using all subject data combined, the error in mediolateral GRF estimates increased; however, the average error for anterior-posterior and vertical GRF predictions stayed below 5%. An additional subject performed a calibration test by running at seven different speeds to train an ANN model for predicting VGRF curves and three VGRF characteristics (PIF, TPIF, and SD). Once calibrated, the ANN model estimated VGRF curves from three separate test speeds with less than 4% error, and produced correlations with an r greater than 0.90. Similar results were found when estimating VGRF characteristics as opposed to the entire curve. The ability to estimate 3D GRF using NCPF sensors, especially for VGRF over a range of gait speeds, is an essential step towards developing a mobile gait analysis system.

# 5 OVERALL CONCLUSION AND FUTURE WORK

This thesis discussed the implementation and validation of a nanocomposite piezoresponsive foam (NCPF) instrumented shoe to estimate three-dimensional (3D) ground reaction forces (GRF). GRF and sensor data were collected simultaneously while subjects ran on a force-plate instrumented treadmill. Two studies were performed: a multi-subject walking study and a single-subject multi-speed study. For the multi-subject study, nine subjects were recruited to walk for 2 minutes at 3 mph. For the single-subject pilot study, a subject was recruited to run on a treadmill over a range of seven speeds for 30 seconds, after which, that subject ran at three randomly selected speeds for 30 seconds. Two different approaches were used to model GRF using sensor data as inputs: a statistical approach using a functional data analysis (FDA), and a machine learning approach using an artificial neural network (ANN). The multi-subject study data was used to test and compare the statistical approach and the machine learning approach, where 3D GRF models were created for each individual subject as well as a general model using all subject data combined. The single-subject data was used to test the predictive abilities of the machine learning approach, where vertical ground reaction force (VGRF) curves and characteristics were predicted from random gait speeds.

Results from the multi-subject study showed that both statistical and machine learning approaches produced 3D GRF estimates with a high degree of accuracy. Individual FDA models estimated 3D GRF with a minimum error of 1.99%, and individual ANN models estimated 3D

GRF with a minimum error of 0.98%. General FDA models using all subject data combined estimated 3D GRF with a minimum error of 2.51% and general ANN models estimated 3D GRF with a minimum error of 1.70%. Results from the single-subject pilot study showed that ANN models are able to accurately predict VGRF curves and characteristics after calibrating for a range of gait speeds. ANN models were able to predict VGRF curves for three randomly selected speeds with an average error of 3.73%. Another ANN model was able to predict VGRF characteristics for three randomly selected speeds with a minimum error of 5.37%.

The results proved that both statistical and machine learning approaches can be used to estimate 3D GRF using NCPF sensor data as inputs. FDA models produced the most accurate estimates for anterior-posterior and mediolateral GRF, whereas ANN models produced the most accurate estimates for vertical GRF. Creating unique models for each individual subject yielded the highest accuracy, whereas a general model for all subjects produced higher errors. Both approaches were unable to accurately estimate GRF for an out-of-sample subject (e.g. create a model with 8 subjects and predict an entirely new subject); this is understandable considering that the number of subjects used herein does not encapsulate the general gait of the population.

To enable predictions across subjects, it is recommended that future work be focused on gathering a larger sample size of human gait data. The studies presented in this thesis used 10 subjects total, which does not begin to cover the various styles of gait in the population (e.g. heel strike runners, fore-foot strike runners, etc.). Future data collection should recruit a wider variety of subjects to produce more robust models; subjects for this thesis' work were all in their mid-twenties and displayed a small range of height and weight. By collecting a larger array of GRF and NCPF sensor data, subjects may be able to be classified into different categories of gait where generalized models could be developed to estimate 3D GRF for each category.

To improve the accuracy of GRF models for future data collection, especially along the anterior-posterior and mediolateral directions, it is also recommended that the design of the sensor system be optimized. The current design consists of having one NCPF sensor located at four different positions under the insole of the shoe: heel, arch, ball, and toe. Because these sensors are aligned along the anterior-posterior axis, anterior-posterior GRF and vertical GRF are more easily obtained via direct impact during running; whereas, the mediolateral GRF relies on a perpendicular movement across each sensor, which may not be easily obtainable during impact. It is suggested that additional sensors be added along the mediolateral axis of the insole to better capture mediolateral GRF and improve model accuracy. Once the sensor topology has been optimized, tests must be performed that accurately reflect real-life scenarios. Some of these tests include out-of-lab testing (e.g. different surfaces and gradients) as well as testing over longer durations of time relative to normal exercise (e.g. 30 minutes to 2+ hours). These tests may reveal signal drift and mechanical degradation in the sensor, which must be identified and corrected to produce accurate GRF estimates.

Estimating additional data such as ground reaction moments (GRM), center of pressure (COP), and body kinematics is essential to producing a fully mobile system capable of performing gait analysis. The current system presented in this thesis estimates 3D GRF using wearable sensors embedded in the soles of a shoe. To be able to perform a complete gait analysis, GRM, COP, and joint angle data are also required, along with GRF data, to perform an inverse dynamic analysis resulting in joint reaction forces and joint reaction moments. It may be possible to estimate these parameters with NCPF sensors by using a machine learning application; Li et al. used GRF and GRM as inputs into a neural network to estimate knee and hip angles with a high degree of accuracy [50]. This approach could be applied in future work

where NCPF sensors could be used to estimate GRF, GRM, COP, and joint angles via multiple ANN models; thus, a mobile gait analysis could be performed using only NCPF sensors.

An alternative approach for estimating body kinematics is to use wearable sensors attached across the joints of the subject. In the BYU nanocomposites lab, wearable high-deflection strain gauge sensors are currently being developed to estimate joint angles during movement. By combining these sensors with the current NCPF sensors, kinetic and kinematic information could be produced to perform gait analysis. By creating a mesh network of these sensors, it could then be possible to create a mobile gait analysis system capable of providing joint force estimations in real-time, without the need to post-process the data.

Once a mobile gait analysis system has been developed, it is strongly recommended that this system be validated with a clinical application such as knee osteoarthritis (KOA). KOA is the most common form of arthritis in adults [76] and the most common type of joint pain in the United States [77]. Using gait analysis to observe subjects with KOA, it has been shown that they will have a higher vertical loading rate and a reduced range of knee flexion across the entire gait cycle [78-80]. If these same measures could be estimated by a mobile gait analysis system when applied to subjects displaying KOA, then the validity of these sensors could be shown for real-life applications.

In conclusion, the work presented in this thesis shows that NCPF sensors are a feasible solution for estimating 3D GRF. With continued work, it is anticipated that these sensors can be integrated into a mobile gait analysis system. This resulting system will allow clinicians and researchers to gather unprecedented out-of-lab data, which could be used to improve our understanding of human gait.

## REFERENCES


[1] Baker, R., 2007, "The history of gait analysis before the advent of modern computers," Gait & posture, 26(3), pp. 331-342.

[2] Andriacchi, T. P., and Alexander, E. J., 2000, "Studies of human locomotion: past, present and future," Journal of biomechanics, 33(10), pp. 1217-1224.

[3] Weber, W., and Weber, E. F., 1836, Mechanik der menschlichen Gehwerkzeuge: eine anatomisch-physiologische Untersuchung, Dietrich.

[4] Braune, W., and Fischer, O., 1895, Der Gang des Menschen: I. Theil: Versuche am unbelasteten und belasteten Menschen, BS Hirzel.

[5] Gordon, D., Robertson, E., and Winter, D. A., 1980, "Mechanical energy generation, absorption and transfer amongst segments during walking," Journal of biomechanics, 13(10), pp. 845-854.

[6] Ivanenko, Y. P., Poppele, R. E., and Lacquaniti, F., 2004, "Five basic muscle activation patterns account for muscle activity during human locomotion," The Journal of physiology, 556(1), pp. 267-282.

[7] Kadaba, M., Wootten, M., Gainey, J., and Cochran, G., 1985, "Repeatability of phasic muscle activity: performance of surface and intramuscular wire electrodes in gait analysis," Journal of Orthopaedic Research, 3(3), pp. 350-359.

[8] Winter, D. A., and Robertson, D., 1978, "Joit torque and energy patterns in normal gait," Biological Cybernetics, 29(3), pp. 137-142.

[9] Detrembleur, C., Van den Hecke, A., and Dierick, F., 2000, "Motion of the body centre of gravity as a summary indicator of the mechanics of human pathological gait," Gait & posture, 12(3), pp. 243-250.

[10] Iida, H., and Yamamuro, T., 1987, "Kinetic analysis of the center of gravity of the human body in normal and pathological gaits," Journal of biomechanics, 20(10), pp. 987-995.

[11] Shimba, T., 1984, "An estimation of center of gravity from force platform data," Journal of Biomechanics, 17(1), pp. 53-60.

[12] Damiano, D. L., and Abel, M. F., 1996, "Relation of gait analysis to gross motor function in cerebral palsy," Developmental Medicine & Child Neurology, 38(5), pp. 389-396.

[13] Gage, J. R., 1993, "An Essential Tool in the Treatment of Cerebral Palsy," Clinical orthopaedics and related research, 288, pp. 126-134.

[14] Tao, W., Liu, T., Zheng, R., and Feng, H., 2012, "Gait analysis using wearable sensors," Sensors, 12(2), pp. 2255-2283.

[15] D'Angelo, M. G., Berti, M., Piccinini, L., Romei, M., Guglieri, M., Bonato, S., Degrate, A., Turconi, A. C., and Bresolin, N., 2009, "Gait pattern in Duchenne muscular dystrophy," Gait & posture, 29(1), pp. 36-41.

[16] Gaudreault, N., Gravel, D., Nadeau, S., Houde, S., and Gagnon, D., 2010, "Gait patterns comparison of children with Duchenne muscular dystrophy to those of control subjects considering the effect of gait velocity," Gait & posture, 32(3), pp. 342-347.

[17] Sutherland, D. H., Olshen, R., Cooper, L., Wyatt, M., Leach, J., Mubarak, S., and Schultz, P., 1981, "The pathomechanics of gait in Duchenne muscular dystrophy," Developmental Medicine & Child Neurology, 23(1), pp. 3-22.

[18] Givon, U., Zeilig, G., and Achiron, A., 2009, "Gait analysis in multiple sclerosis: characterization of temporal–spatial parameters using GAITRite functional ambulation system," Gait & posture, 29(1), pp. 138-142.

[19] Valderrabano, V., Nigg, B. M., von Tscharner, V., Stefanyshyn, D. J., Goepfert, B., and Hintermann, B., 2007, "Gait analysis in ankle osteoarthritis and total ankle replacement," Clinical Biomechanics, 22(8), pp. 894-904.

[20] Olney, S. J., Griffin, M. P., and McBride, I. D., 1998, "Multivariate examination of data from gait analysis of persons with stroke," Physical Therapy, 78(8), pp. 814-828.

[21] Olney, S. J., GrifJin, M. P., Monga, T. N., and McBride, I. D., 1991, "Work and power in gait of stroke patients," Knee, 1, p. H2.

[22] Arendt-Nielsen, L., Graven-Nielsen, T., Svarrer, H., and Svensson, P., 1996, "The influence of low back pain on muscle activity and coordination during gait: a clinical and experimental study," Pain, 64(2), pp. 231-240.

[23] Zijlmans, J., Poels, P., Duysens, J., Van der Straaten, J., Thien, T., Van't Hof, M., Thijssen, H., and Horstink, M., 1996, "Quantitative gait analysis in patients with vascular parkinsonism," Movement Disorders, 11(5), pp. 501-508.

[24] Whittle, M. W., 1996, "Clinical gait analysis: A review," Human Movement Science, 15(3), pp. 369-387.

[25] Sutherland, D. H., 2005, "The evolution of clinical gait analysis part III–kinetics and energy assessment," Gait & Posture, 21(4), pp. 447-461.

[26] Beckett, R., and Chang, K., 1968, "An evaluation of the kinematics of gait by minimum energy," Journal of Biomechanics, 1(2), pp. 147-159.

[27] Sutherland, D. H., 2002, "The evolution of clinical gait analysis: Part II Kinematics," Gait & posture, 16(2), pp. 159-179.

[28] Sutherland, D. H., 2001, "The evolution of clinical gait analysis part l: kinesiological EMG," Gait & posture, 14(1), pp. 61-70.

[29] Popp, K. L., McDermott, W., Hughes, J. M., Baxter, S. A., Stovitz, S. D., and Petit, M. A., 2017, "Bone strength estimates relative to vertical ground reaction force discriminates women runners with stress fracture history," Bone, 94, pp. 22-28.

[30] Crowell, H. P., and Davis, I. S., 2011, "Gait retraining to reduce lower extremity loading in runners," Clinical biomechanics, 26(1), pp. 78-83.

[31] Lieberman, D. E., Venkadesan, M., Werbel, W. A., Daoud, A. I., D'Andrea, S., Davis, I. S., Mang'Eni, R. O., and Pitsiladis, Y., 2010, "Foot strike patterns and collision forces in habitually barefoot versus shod runners," Nature, 463(7280), pp. 531-535.

[32] Daoud, A. I., Geissler, G. J., Wang, F., Saretsky, J., Daoud, Y. A., and Lieberman, D. E., 2012, "Foot strike and injury rates in endurance runners: a retrospective study," Medicine and science in sports and exercise, 44(7), pp. 1325-1334.

[33] Dai, B., Butler, R., Garrett, W., and Queen, R., 2014, "Using ground reaction force to predict knee kinetic asymmetry following anterior cruciate ligament reconstruction," Scandinavian journal of medicine & science in sports, 24(6), pp. 974-981.

[34] Heise, G. D., and Martin, P. E., 2001, "Are variations in running economy in humans associated with ground reaction force characteristics?," European Journal of Applied Physiology, 84(5), pp. 438-442.

[35] Simon, S. R., 2004, "Quantification of human motion: gait analysis—benefits and limitations to its application to clinical problems," Journal of biomechanics, 37(12), pp. 1869-1880.

[36] Wren, T. A., Gorton, G. E., Ounpuu, S., and Tucker, C. A., 2011, "Efficacy of clinical gait analysis: A systematic review," Gait & posture, 34(2), pp. 149-153.

[37] Xu, W., Huang, M.-C., Amini, N., Liu, J. J., He, L., and Sarrafzadeh, M., "Smart insole: a wearable system for gait analysis," Proc. Proceedings of the 5th International Conference on PErvasive Technologies Related to Assistive Environments, ACM, p. 18.

[38] Ramanathan, A. K., Kiran, P., Arnold, G. P., Wang, W., and Abboud, R. J., 2010, "Repeatability of the Pedar-X ® in-shoe pressure measuring system," Foot Ankle Surg, 16.

[39] Khurelbaatar, T., Kim, K., Lee, S., and Kim, Y. H., 2015, "Consistent accuracy in whole-body joint kinetics during gait using wearable inertial motion sensors and in-shoe pressure sensors," Gait & Posture, 42(1), pp. 65-69.

[40] Rouhani, H., Favre, J., Crevoisier, X., and Aminian, K., 2010, "Ambulatory assessment of 3D ground reaction force using plantar pressure distribution," Gait & Posture, 32(3), pp. 311-316.

[41] Rouhani, H., Favre, J., Crevoisier, X., and Aminian, K., 2014, "A wearable system for multi-segment foot kinetics measurement," Journal of Biomechanics, 47(7), pp. 1704-1711.

[42] Oerbekke, M. S., Stukstette, M. J., Schütte, K., de Bie, R. A., Pisters, M. F., and Vanwanseele, B., 2017, "Concurrent validity and reliability of wireless instrumented insoles measuring postural balance and temporal gait parameters," Gait & Posture, 51, pp. 116-124.

[43] Jacobs, D. A., and Ferris, D. P., 2015, "Estimation of ground reaction forces and ankle moment with multiple, low-cost sensors," Journal of NeuroEngineering and Rehabilitation, 12(1), pp. 1-12.

[44] Crea, S., Donati, M., De Rossi, S. M. M., Oddo, C. M., and Vitiello, N., 2014, "A wireless flexible sensorized insole for gait analysis," Sensors, 14(1), pp. 1073-1093.

[45] Howell, A. M., Kobayashi, T., Hayes, H. A., Foreman, K. B., and Bamberg, S. J., 2013, "Kinetic gait analysis using a low-cost insole," Biomedical Engineering, IEEE Transactions on, 60(12), pp. 3284-3290.

[46] González, I., Fontecha, J., Hervás, R., and Bravo, J., 2015, "An ambulatory system for gait monitoring based on wireless sensorized insoles," Sensors, 15(7), pp. 16589-16613.

[47] Minto, S., Zanotto, D., Boggs, E. M., Rosati, G., and Agrawal, S. K., 2016, "Validation of a Footwear-Based Gait Analysis System With Action-Related Feedback," IEEE Transactions on Neural Systems and Rehabilitation Engineering, 24(9), pp. 971-980.

[48] Liu, T., Inoue, Y., and Shibata, K., 2010, "A wearable force plate system for the continuous measurement of triaxial ground reaction force in biomechanical applications," Measurement Science and Technology, 21(8), p. 085804.

[49] Liu, T., Inoue, Y., Shibata, K., Shiojima, K., and Han, M. M., 2014, "Triaxial joint moment estimation using a wearable three-dimensional gait analysis system," Measurement, 47, pp. 125-129.

[50] Li, G., Liu, T., Yi, J., Wang, H., Li, J., and Inoue, Y., 2016, "The Lower Limbs Kinematics Analysis by Wearable Sensor Shoes," IEEE Sensors Journal, 16(8), pp. 2627-2638.

[51] Fluit, R., Andersen, M. S., Kolk, S., Verdonschot, N., and Koopman, H., 2014, "Prediction of ground reaction forces and moments during various activities of daily living," Journal of biomechanics, 47(10), pp. 2321-2329.

[52] Faber, G., Chang, C., Kingma, I., Dennerlein, J., and van Dieën, J., 2016, "Estimating 3D L5/S1 moments and ground reaction forces during trunk bending using a full-body ambulatory inertial motion capture system," Journal of biomechanics, 49(6), pp. 904-912.

[53] Oh, S. E., Choi, A., and Mun, J. H., 2013, "Prediction of ground reaction forces during gait based on kinematics and a neural network model," Journal of biomechanics, 46(14), pp. 2372-2380.

[54] Liu, T., Inoue, Y., and Shibata, K., 2009, "Development of a wearable sensor system for quantitative gait analysis," Measurement, 42(7), pp. 978-988.

[55] Bergmann, J., and McGregor, A., 2011, "Body-worn sensor design: what do patients and clinicians want?," Annals of biomedical engineering, 39(9), pp. 2299-2312.

[56] Johnson, O. K., Gardner, C. J., Fullwood, D. T., Adams, B. L., Hansen, N., and Hansen, G., 2010, "The colossal piezoresistive effect in nickel nanostrand polymer composites and a quantum tunneling model," Computers, Materials, & Continua, 15(2), pp. 87-112.

[57] Baradoy, D. A., 2015, "Composition Based Modaling of Silicone Nano-Composite Strain Gauges."

[58] Johnson, O. K., Kaschner, G. C., Mason, T. A., Fullwood, D. T., and Hansen, G., 2011, "Optimization of nickel nanocomposite for large strain sensing applications," Sensors and Actuators A: Physical, 166(1), pp. 40-47.

[59] Bilodeau, R. A., Fullwood, D. T., Colton, J. S., Yeager, J. D., Bowden, A. E., and Park, T., 2015, "Evolution of nano-junctions in piezoresistive nanostrand composites," Composites Part B: Engineering, 72, pp. 45-52.

[60] Athanasopoulos, N., Baltopoulos, A., Matzakou, M., Vavouliotis, A., and Kostopoulos, V., 2012, "Electrical conductivity of polyurethane/MWCNT nanocomposite foams," Polymer Composites, 33(8), pp. 1302-1312.

[61] Merrell, A. J., Fullwood, D. T., Bowden, A. E., Remington, T. D., Stolworthy, D. K., and Bilodeau, A., "Applications of Nano-Composite Piezoelectric Foam Sensors," Proc. ASME 2013 Conference on Smart Materials, Adaptive Structures and Intelligent Systems, American Society of Mechanical Engineers, pp. V001T001A024-V001T001A024.

[62] Bird, E. T., Merrell, A. J., Anderson, B. K., Newton, C. N., Rosquist, P. G., Fullwood, D. T., Bowden, A. E., and Seeley, M. K., 2016, "Vibration monitoring via nano-composite piezoelectric foam bushings," Smart Materials and Structures, 25(11), p. 115013.

[63] Johnson, O. K., Gardner, C. J., Seegmiller, D. B., Mara, N. A., Dattelbaum, A. M., Rae, P. J., Kaschner, G. C., Mason, T. A., Fullwood, D. T., and Hansen, G., 2011, "Multiscale model for the extreme piezoresistivity in silicone/nickel nanostrand nanocomposites," Metallurgical and Materials Transactions A, 42(13), pp. 3898-3906.

[64] Cuevas, A., 2014, "A partial overview of the theory of statistics with functional data," Journal of Statistical Planning and Inference, 147, pp. 1-23.

[65] Du, J., and Xu, Y., 2017, "Hierarchical deep neural network for multivariate regression," Pattern Recognition, 63, pp. 149-157.

[66] Faber, G. S., Kingma, I., Schepers, H. M., Veltink, P. H., and Van Dieen, J. H., 2010, "Determination of joint moments with instrumented force shoes in a variety of tasks," Journal of biomechanics, 43(14), pp. 2848-2854.

[67] Bird, E. M., AJ; Anderson, B; Newton, C; Rosquist, P; Fullwood, D; Bowden, A; Seeley, M, 2016, "Vibration Monitoring via Nanocomposite Piezoelectric Foam Bushings," Smart Materials and Structures, In Press.

[68] Gage, J. R., Deluca, P. A., and Renshaw, T. S., 1995, "Gait analysis: principles and applications," The Journal of Bone & Joint Surgery, 77(10), pp. 1607-1623.

[69] Team, R. C., 2015, "R: A language and environment for statistical computing [Internet]. Vienna, Austria: R Foundation for Statistical Computing; 2013," Document freely available on the internet at: http://www. r-project. org.

[70] Giakas, G., and Baltzopoulos, V., 1997, "Time and frequency domain analysis of ground reaction forces during walking: an investigation of variability and symmetry," Gait & Posture, 5(3), pp. 189-197.

[71] Munro, C. F., Miller, D. I., and Fuglevand, A. J., 1987, "Ground reaction forces in running: a reexamination," Journal of biomechanics, 20(2), pp. 147-155.

[72] Rosquist, P. G., Collins, G., Merrell, A. J., Tuttle, N. J., Tracy, J. B., Bird, E. T., Seeley, M. K., Fullwood, D. T., Christensen, W. F., and Bowden, A. E., 2017, "Estimation of 3D Ground Reaction Force Using Nanocomposite Piezo-Responsive Foam Sensors During Walking," Annals of Biomedical Engineering, pp. 1-13.

[73] Beale, M. H., Hagan, M. T., and Demuth, H. B., 1992, "Neural Network Toolbox™ Getting Started Guide."

[74] Weyand, P. G., Sternlight, D. B., Bellizzi, M. J., and Wright, S., 2000, "Faster top running speeds are achieved with greater ground forces not more rapid leg movements," Journal of applied physiology, 89(5), pp. 1991-1999.

[75] Jung, S.-K., and McDonald, K., 2011, "Visual gene developer: a fully programmable bioinformatics software for synthetic gene optimization," Bmc Bioinformatics, 12(1), p. 340.

[76] Michael, J. W.-P., Schlüter-Brust, K. U., and Eysel, P., 2010, "The epidemiology, etiology, diagnosis, and treatment of osteoarthritis of the knee," Deutsches Arzteblatt International, 107(9), p. 152.

[77] Zhang, Y., and Jordan, J. M., 2010, "Epidemiology of Osteoarthritis," Clinics in geriatric medicine, 26(3), pp. 355-369.

[78] Deluzio, K., and Astephen, J., 2007, "Biomechanical features of gait waveform data associated with knee osteoarthritis: an application of principal component analysis," Gait & posture, 25(1), pp. 86-93.

[79] Andriacchi, T. P., Galante, J. O., and Fermier, R. W., 1982, "The influence of total knee-replacement design on walking and stair-climbing," The Journal of bone and joint surgery. American volume, 64(9), pp. 1328-1335.

[80] Schnitzer, T. J., Popovich, J. M., Andersson, G. B., and Andriacchi, T. P., 1993, "Effect of piroxicam on gait in patients with osteoarthritis of the knee," Arthritis & Rheumatism, 36(9), pp. 1207-1213.

## APPENDIX A. SINGLE SUBJECT STATISTICAL MODELS

**Table A-I: Reported absolute error (MAE), absolute percent error (MAPE), standard deviation of absolute error (SDAE) and number of amplitudes (K) of the optimal round reaction force (GRF) single subject (SS) model for each subject. All errors are calculated from cross-validation.**

| Subject | Anterior-posterior | | | | Medial-lateral | | | | Vertical | | | |
|---|---|---|---|---|---|---|---|---|---|---|---|---|
| | MAE (N) | MAPE (%) | SDAE (N) | K | MAE (N) | MAPE (%) | SDAE (N) | K | MAE (N) | MAPE (%) | SDAE (N) | K |
| **1** | 4.55 | 1.85 | 4.09 | 28 | 4.28 | 6.33 | 4.37 | 32 | 11.73 | 1.91 | 11.28 | 26 |
| **2** | 6.52 | 1.96 | 5.41 | 20 | 5.20 | 6.40 | 4.61 | 14 | 16.88 | 1.89 | 12.93 | 18 |
| **3** | 7.31 | 2.38 | 7.73 | 16 | 5.53 | 10.30 | 5.09 | 16 | 13.42 | 2.00 | 12.20 | 22 |
| **4** | 6.60 | 1.89 | 5.96 | 20 | 4.22 | 5.22 | 3.95 | 20 | 15.19 | 2.12 | 14.44 | 14 |
| **5** | 8.89 | 2.34 | 7.38 | 20 | 5.64 | 6.26 | 4.79 | 16 | 23.99 | 2.56 | 22.91 | 16 |
| **6** | 8.88 | 2.32 | 8.36 | 24 | 4.99 | 6.43 | 4.42 | 16 | 18.45 | 2.47 | 18.45 | 18 |
| **7** | 5.79 | 1.66 | 5.16 | 16 | 5.17 | 6.02 | 4.54 | 16 | 14.16 | 1.81 | 13.88 | 16 |
| **8** | 4.62 | 1.56 | 4.42 | 26 | 3.43 | 5.89 | 3.13 | 20 | 8.96 | 1.65 | 8.75 | 20 |
| **9** | 5.54 | 1.98 | 4.62 | 24 | 4.61 | 5.15 | 3.79 | 20 | 16.09 | 2.27 | 14.60 | 20 |

**Table A-II: Reported absolute error (MAE), absolute percent error (MAPE), standard deviation of absolute error (SDAE) and number of amplitudes (K) of the optimal ground reaction force (GRF) estimates from the combined-subject voltage (CSV) model for each test subject. All errors are calculated from cross-validation.**

| Test Subject | Anterior-posterior | | | | Medial-lateral | | | | Vertical | | | |
|---|---|---|---|---|---|---|---|---|---|---|---|---|
| | MAE (N) | MAPE (%) | SDAE (N) | K | MAE (N) | MAPE (%) | SDAE (N) | K | MAE (N) | MAPE (%) | SDAE (N) | K |
| **1** | 48.41 | 19.62 | 32.65 | 66 | 14.96 | 21.22 | 11.02 | 66 | 95.55 | 15.75 | 60.94 | 78 |
| **2** | 18.70 | 5.59 | 13.38 | 66 | 40.49 | 46.57 | 14.16 | 66 | 152.66 | 15.51 | 85.46 | 78 |
| **3** | 16.30 | 5.28 | 11.30 | 66 | 36.17 | 67.57 | 17.85 | 66 | 38.03 | 5.81 | 33.35 | 78 |
| **4** | 21.12 | 6.04 | 13.21 | 66 | 40.51 | 49.18 | 15.05 | 66 | 44.24 | 5.82 | 36.48 | 78 |
| **5** | 33.16 | 8.68 | 19.46 | 66 | 46.22 | 49.51 | 19.90 | 66 | 63.01 | 6.56 | 49.09 | 78 |
| **6** | 34.99 | 9.10 | 28.48 | 66 | 10.94 | 13.48 | 10.07 | 66 | 73.90 | 9.46 | 57.13 | 78 |
| **7** | 51.42 | 14.81 | 34.51 | 66 | 95.75 | 109.57 | 38.36 | 66 | 105.32 | 13.99 | 75.80 | 78 |
| **8** | 12.46 | 4.21 | 9.37 | 66 | 9.86 | 15.71 | 7.48 | 66 | 58.80 | 10.57 | 36.93 | 78 |
| **9** | 24.17 | 8.64 | 18.08 | 66 | 38.30 | 41.14 | 18.29 | 66 | 48.27 | 6.63 | 37.89 | 78 |

**Table A-III: Reported absolute error (MAE), absolute percent error (MAPE), standard deviation of absolute error (SDAE) and number of amplitudes (K) of the optimal ground reaction force (GRF) estimates from the combined-subject voltage and demographics (CSVD) model for each test subject. The optimal subject demographics used with sensor data as covariates for creating the CSVD model are listed for each GRF direction. All errors are calculated from cross-validation.**

| Test Subject | Anterior-posterior - Weight | | | | Mediolateral – Gender, Height | | | | Vertical - Weight | | | |
|---|---|---|---|---|---|---|---|---|---|---|---|---|
| | MAE (N) | MAPE (%) | SDAE (N) | K | MAE (N) | MAPE (%) | SDAE (N) | K | MAE (N) | MAPE (%) | SDAE (N) | K |
| **1** | 69.69 | 28.19 | 41.59 | 66 | 22.13 | 31.46 | 13.99 | 66 | 42.87 | 6.94 | 34.82 | 78 |
| **2** | 40.17 | 12.03 | 31.79 | 66 | 18.09 | 20.71 | 11.91 | 66 | 74.09 | 7.82 | 68.00 | 78 |
| **3** | 14.10 | 4.58 | 12.42 | 66 | 39.57 | 74.50 | 24.39 | 66 | 45.56 | 7.01 | 32.84 | 78 |
| **4** | 29.98 | 8.57 | 21.60 | 66 | 67.81 | 82.35 | 26.24 | 66 | 42.69 | 5.62 | 31.08 | 78 |
| **5** | 75.33 | 19.69 | 52.08 | 66 | 30.62 | 33.13 | 17.21 | 66 | 79.06 | 8.16 | 67.97 | 78 |
| **6** | 44.23 | 11.52 | 32.57 | 66 | 17.48 | 21.57 | 12.24 | 66 | 69.47 | 0.08 | 63.33 | 78 |
| **7** | 54.17 | 15.59 | 43.00 | 66 | 39.19 | 44.52 | 20.81 | 66 | 145.30 | 17.94 | 113.96 | 78 |
| **8** | 17.31 | 5.85 | 12.80 | 66 | 24.03 | 38.37 | 16.90 | 66 | 41.19 | 7.21 | 39.22 | 78 |
| **9** | 21.07 | 7.52 | 15.57 | 66 | 30.03 | 32.25 | 23.66 | 66 | 43.26 | 5.96 | 32.23 | 78 |

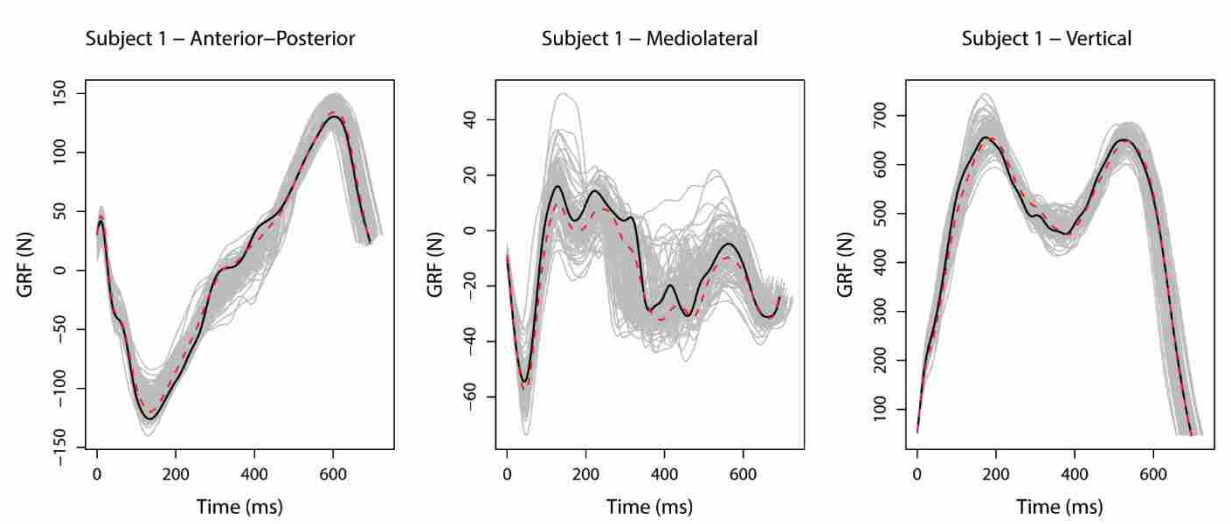


**Figure A-1: Graphs of 3D GRF for subject 1, where the light grey lines represent each individual stance, the solid black line represents one randomly selected actual stance, and the dotted line represents the predicted curve from the Single Subject GRF model corresponding to the actual stance (black line).**

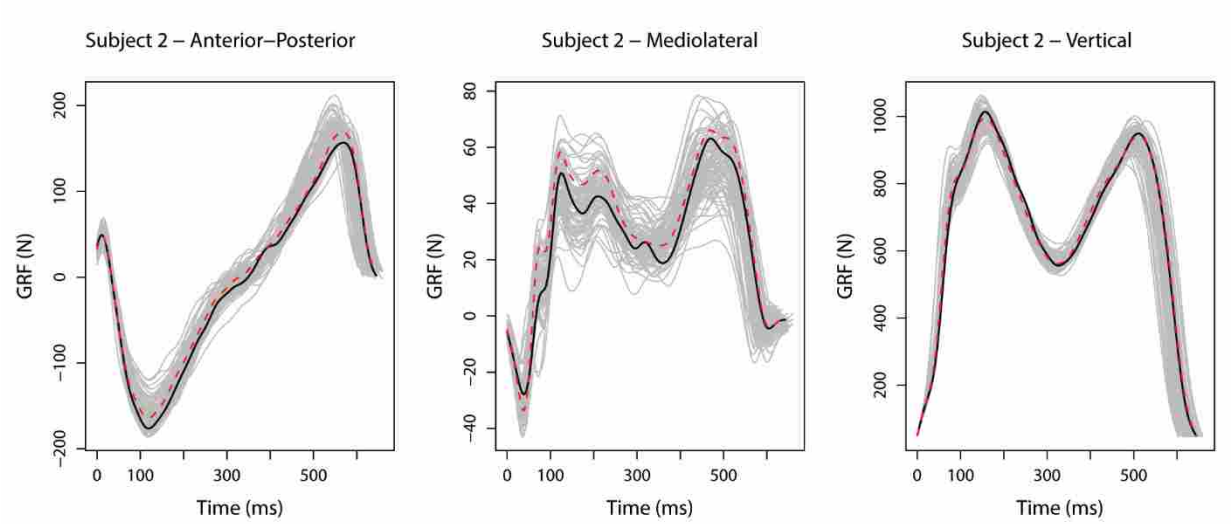


**Figure A-2: Graphs of 3D GRF for subject 2, where the light grey lines represent each individual stance, the solid black line represents one randomly selected actual stance, and the dotted line represents the predicted curve from the Single Subject GRF model corresponding to the actual stance (black line).**

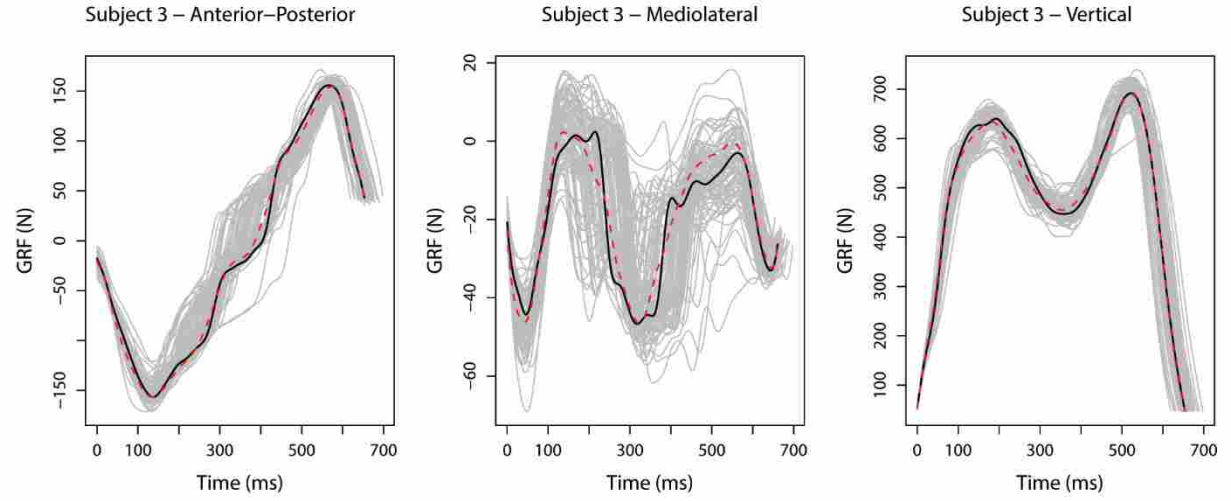


**Figure A-3: Graphs of 3D GRF for subject 3, where the light grey lines represent each individual stance, the solid black line represents one randomly selected actual stance, and the dotted line represents the predicted curve from the Single Subject GRF model corresponding to the actual stance (black line).**

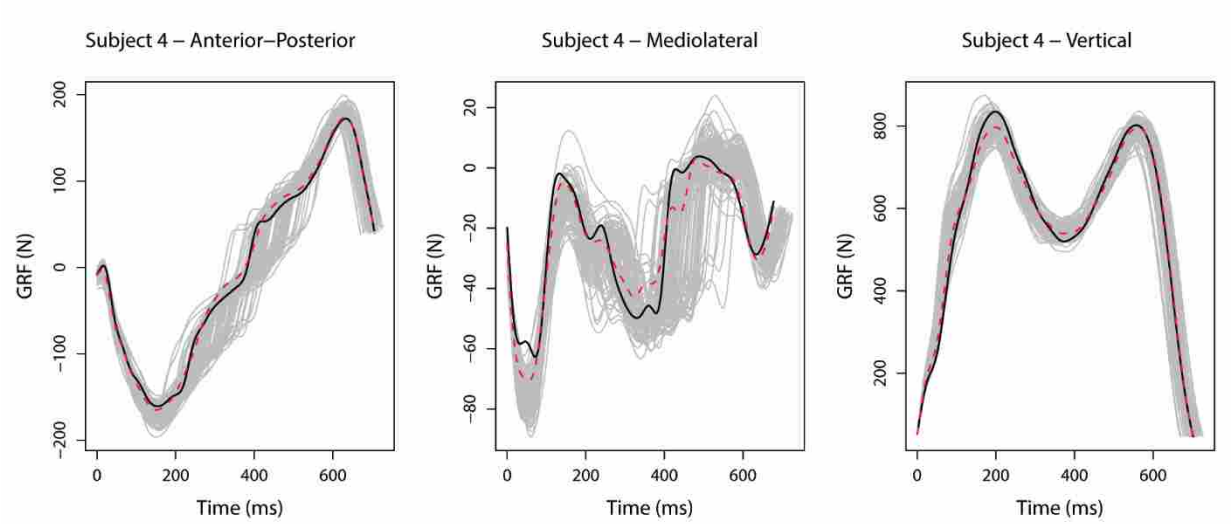


**Figure A-4: Graphs of 3D GRF for subject 4, where the light grey lines represent each individual stance, the solid black line represents one randomly selected actual stance, and the dotted line represents the predicted curve from the Single Subject GRF model corresponding to the actual stance (black line).**

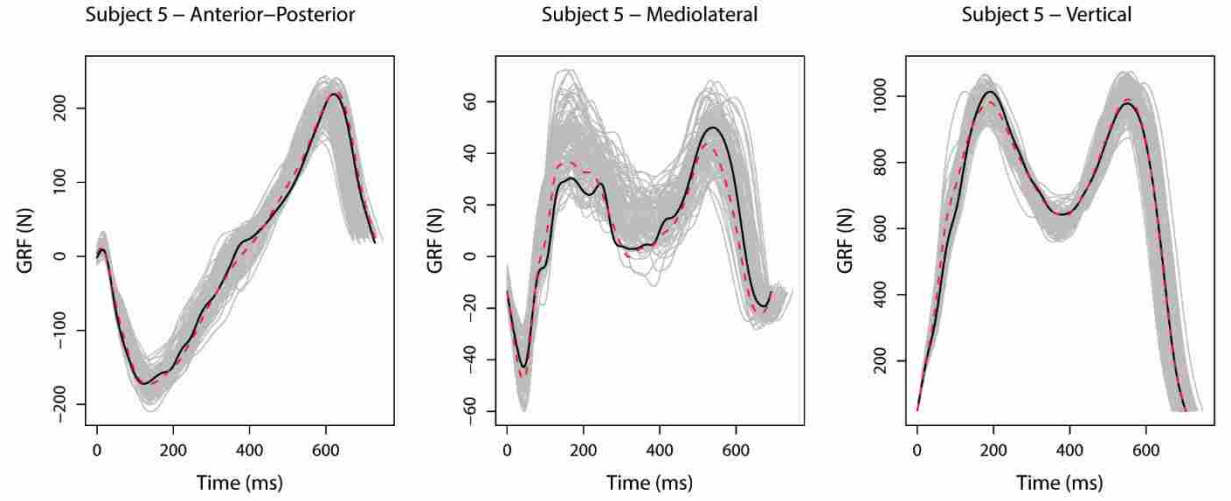


**Figure A-5: Graphs of 3D GRF for subject 5, where the light grey lines represent each individual stance, the solid black line represents one randomly selected actual stance, and the dotted line represents the predicted curve from the Single Subject GRF model corresponding to the actual stance (black line).**

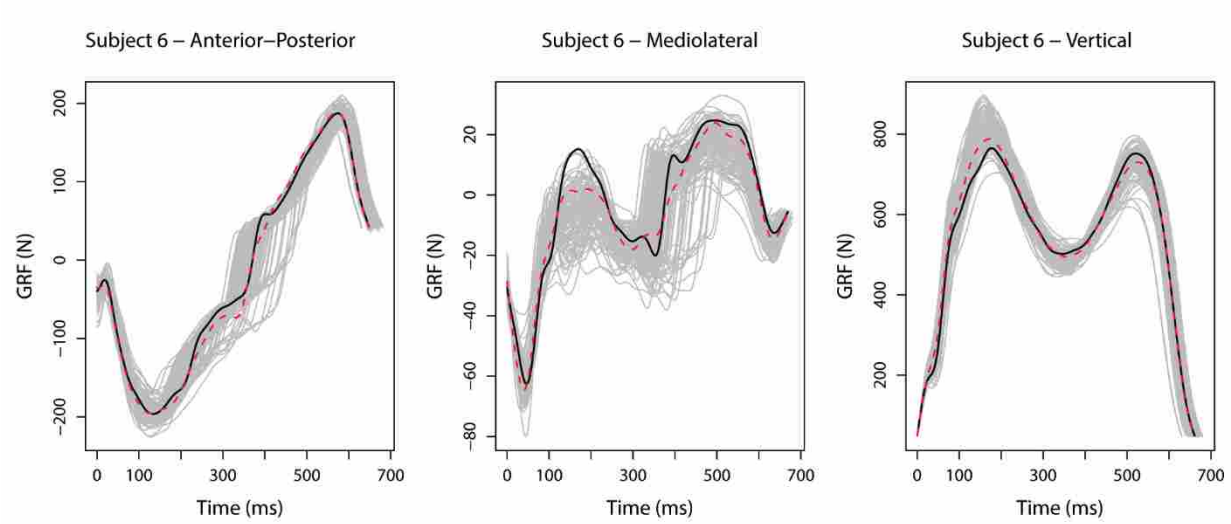


**Figure A-6: Graphs of 3D GRF for subject 6, where the light grey lines represent each individual stance, the solid black line represents one randomly selected actual stance, and the dotted line represents the predicted curve from the Single Subject GRF model corresponding to the actual stance (black line).**

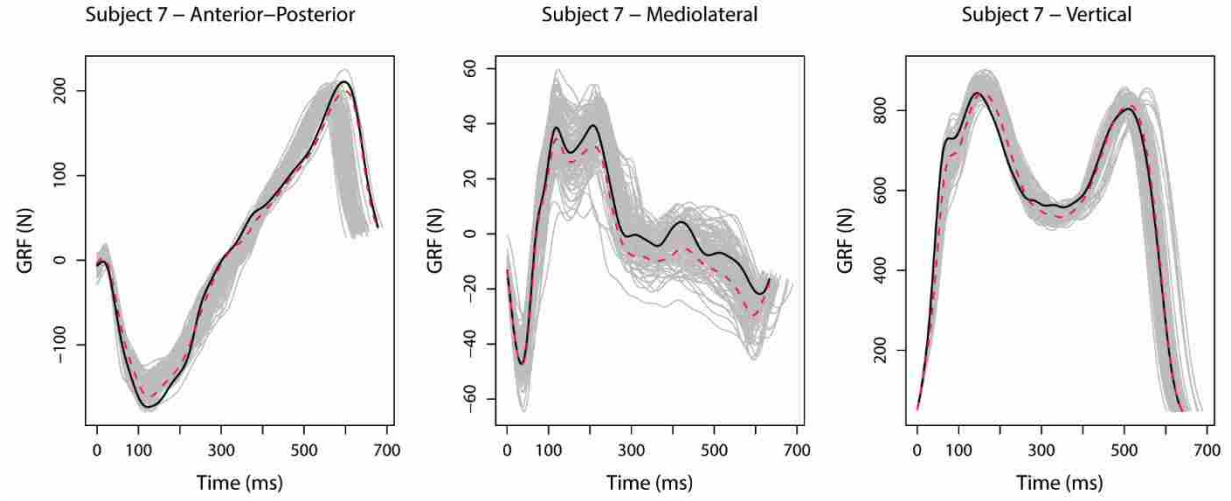


**Figure A-7: Graphs of 3D GRF for subject 7, where the light grey lines represent each individual stance, the solid black line represents one randomly selected actual stance, and the dotted line represents the predicted curve from the Single Subject GRF model corresponding to the actual stance (black line).**

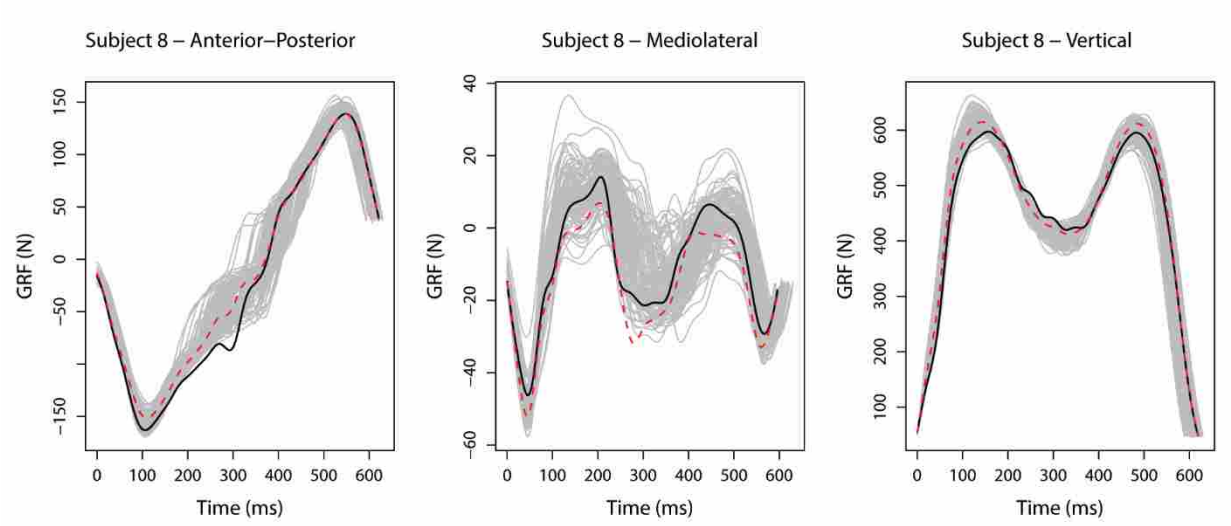


**Figure A-8: Graphs of 3D GRF for subject 8, where the light grey lines represent each individual stance, the solid black line represents one randomly selected actual stance, and the dotted line represents the predicted curve from the Single Subject GRF model corresponding to the actual stance (black line).**

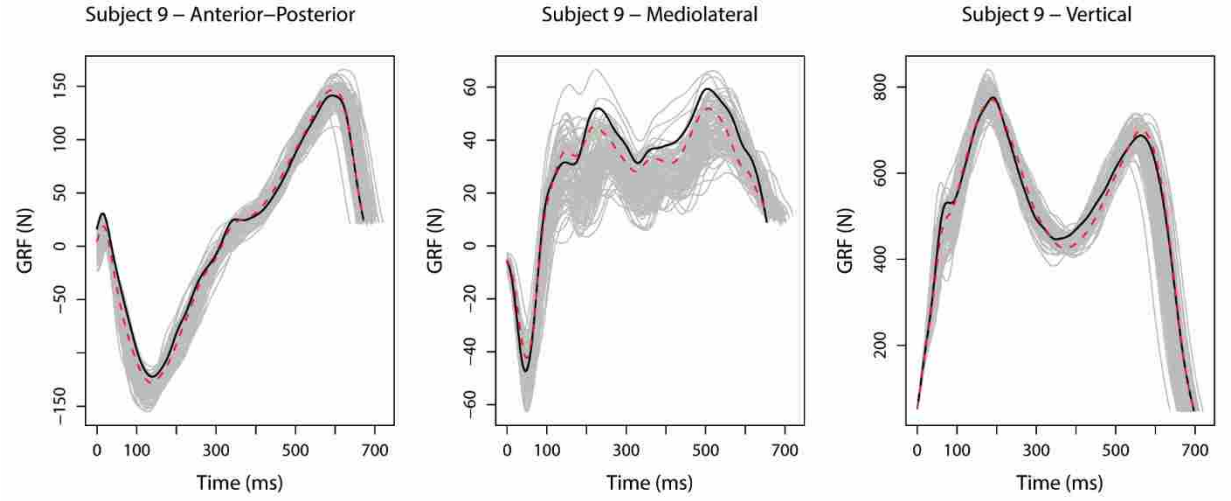


**Figure A-9: Graphs of 3D GRF for subject 9, where the light grey lines represent each individual stance, the solid black line represents one randomly selected actual stance, and the dotted line represents the predicted curve from the Single Subject GRF model corresponding to the actual stance (black line).**

## APPENDIX B. SINGLE SUBJECT ARTIFICIAL NEURAL NETWORK MODELS

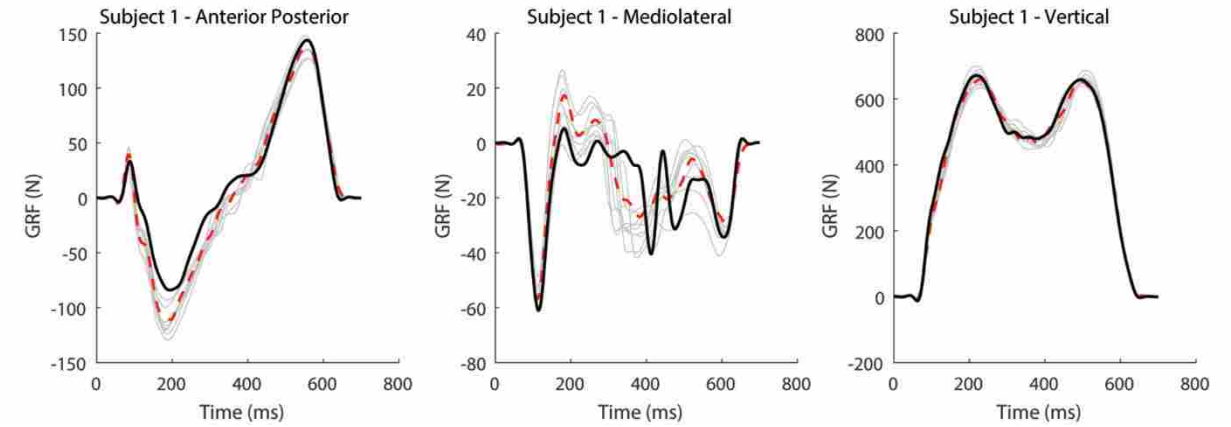


**Figure B-1: Graphs of 3D ground reaction force (GRF) for subject 1 during walking. The grey lines represent GRF curves for each test stance phase, the solid black line represents one randomly selected actual GRF curve, and the dotted red line represents the predicted GRF curve corresponding to the actual GRF curve.**

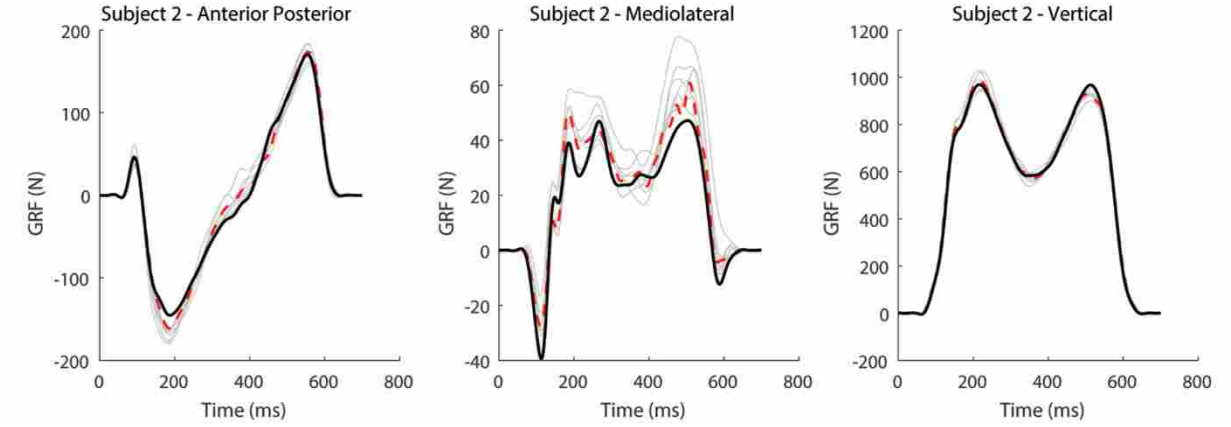


**Figure B-2: Graphs of 3D ground reaction force (GRF) for subject 2 during walking. The grey lines represent GRF curves for each test stance phase, the solid black line represents one randomly selected actual GRF curve, and the dotted red line represents the predicted GRF curve corresponding to the actual GRF curve.**

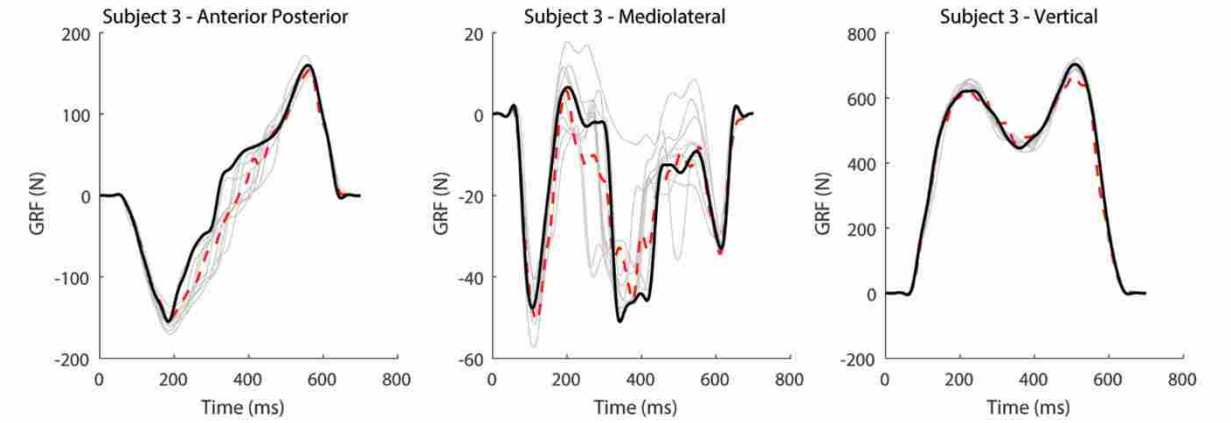


**Figure B-3: Graphs of 3D ground reaction force (GRF) for subject 3 during walking. The grey lines represent GRF curves for each test stance phase, the solid black line represents one randomly selected actual GRF curve, and the dotted red line represents the predicted GRF curve corresponding to the actual GRF curve.**

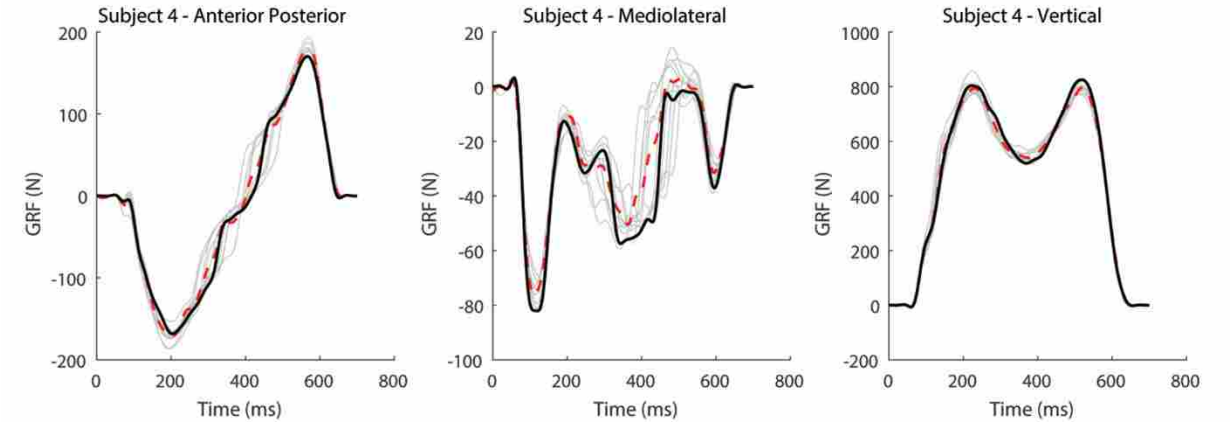


**Figure B-4: Graphs of 3D ground reaction force (GRF) for subject 4 during walking. The grey lines represent GRF curves for each test stance phase, the solid black line represents one randomly selected actual GRF curve, and the dotted red line represents the predicted GRF curve corresponding to the actual GRF curve.**

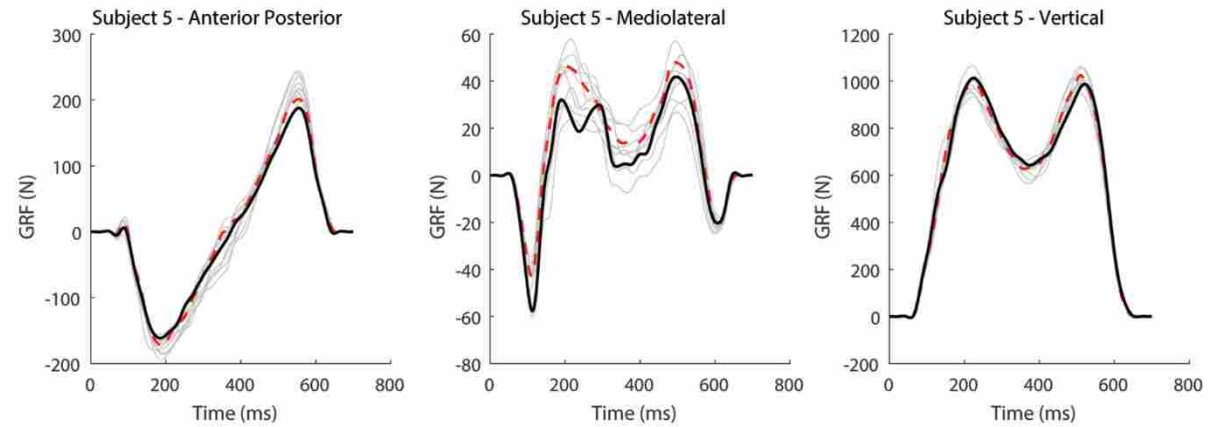


**Figure B-5: Graphs of 3D ground reaction force (GRF) for subject 5 during walking. The grey lines represent GRF curves for each test stance phase, the solid black line represents one randomly selected actual GRF curve, and the dotted red line represents the predicted GRF curve corresponding to the actual GRF curve.**

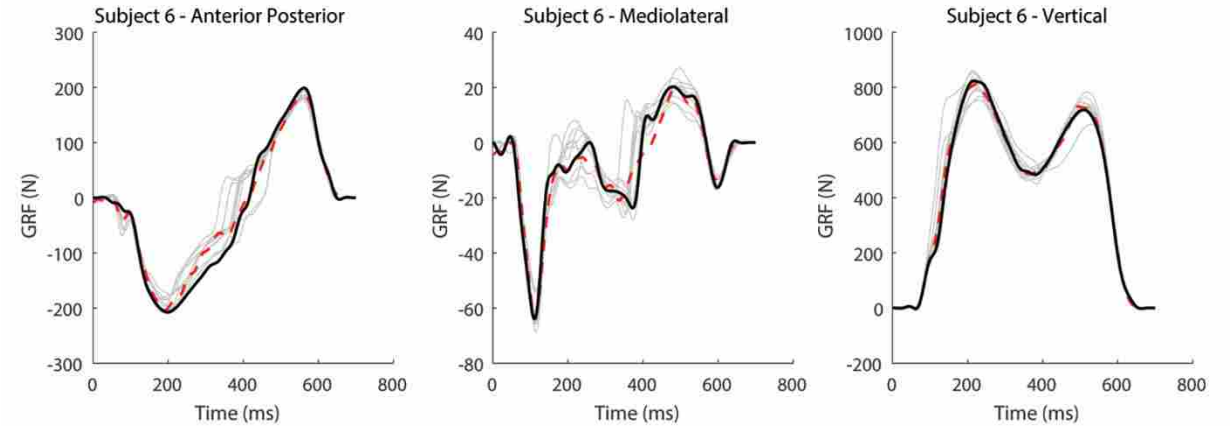


**Figure B-6: Graphs of 3D ground reaction force (GRF) for subject 6 during walking. The grey lines represent GRF curves for each test stance phase, the solid black line represents one randomly selected actual GRF curve, and the dotted red line represents the predicted GRF curve corresponding to the actual GRF curve.**

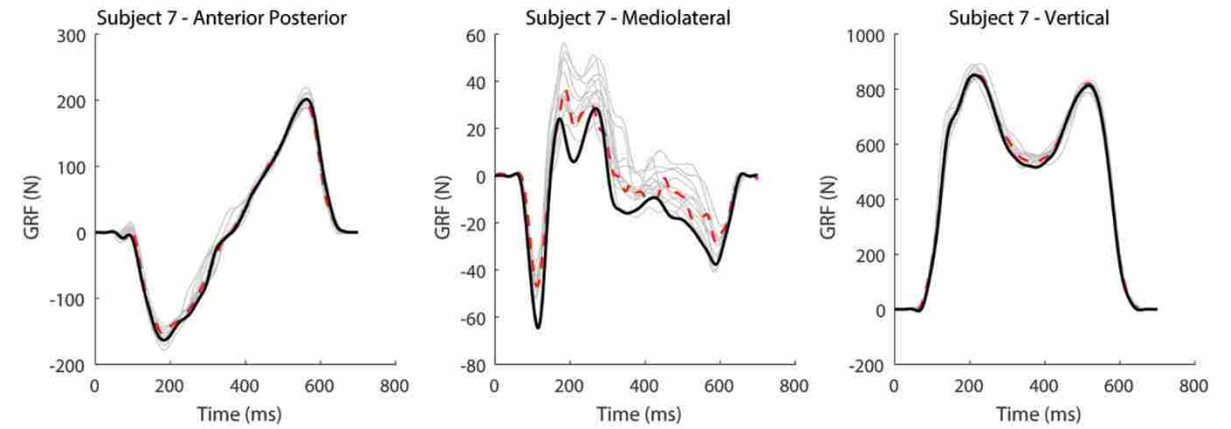


**Figure B-7: Graphs of 3D ground reaction force (GRF) for subject 7 during walking. The grey lines represent GRF curves for each test stance phase, the solid black line represents one randomly selected actual GRF curve, and the dotted red line represents the predicted GRF curve corresponding to the actual GRF curve.**

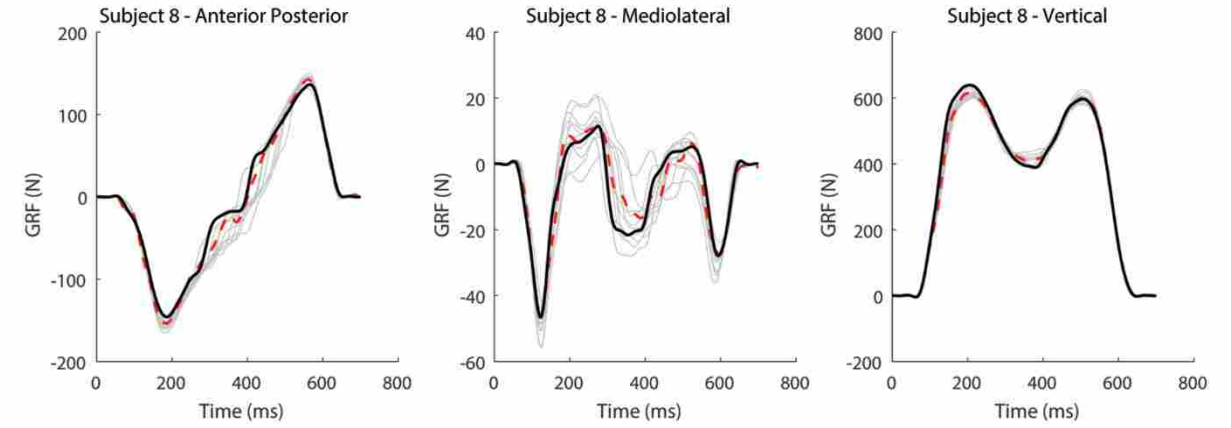


**Figure B-8: Graphs of 3D ground reaction force (GRF) for subject 8 during walking. The grey lines represent GRF curves for each test stance phase, the solid black line represents one randomly selected actual GRF curve, and the dotted red line represents the predicted GRF curve corresponding to the actual GRF curve.**

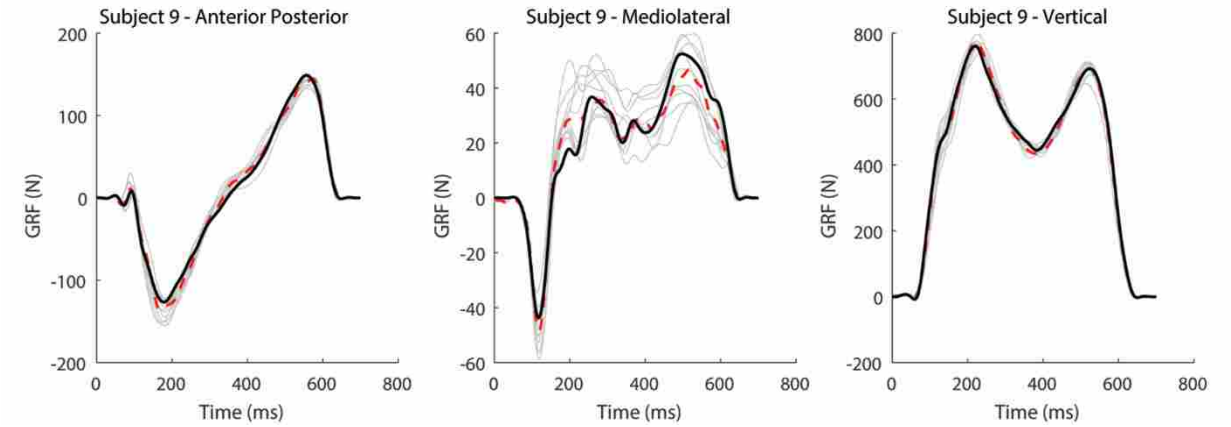


**Figure B-9: Graphs of 3D ground reaction force (GRF) for subject 9 during walking. The grey lines represent GRF curves for each test stance phase, the solid black line represents one randomly selected actual GRF curve, and the dotted red line represents the predicted GRF curve corresponding to the actual GRF curve.**